Enhanced prediction of breast cancer patient response to chemotherapy by integrating deconvolved expression patterns of immune, stromal and tumor cells

Saugato Rahman Dhruba[1], Sahil Sahni[1], Binbin Wang[1], Di Wu[2,3], Padma Sheila Rajagopal[1,4], Yael Schmidt[1], Eldad D. Shulman[1], Sanju Sinha[1,5], Stephen-John Sammut[6,7], Carlos Caldas[8,9], Kun Wang[1,10,11,12,*], Eytan Ruppin[1,*]

[1] Cancer Data Science Laboratory, Center for Cancer Research, National Cancer Institute, National Institutes of Health, Bethesda, MD, USA.

[2] Laboratory of Pathology, Center for Cancer Research, National Cancer Institute, National Institutes of Health, Bethesda, MD, USA.

[3] Department of Pathobiology, University of Illinois Urbana-Champaign, Urbana, IL, USA.

[4] Women's Malignancies Branch, Center for Cancer Research, National Cancer Institute, National Institutes of Health, Bethesda, MD, USA.

[5] NCI-Designated Cancer Center, Sanford Burnham Prebys Medical Discovery Institute, San Diego, CA, USA.

[6] Breast Cancer Now Toby Robins Research Centre, The Institute of Cancer Research, London, UK.

[7] The Royal Marsden Hospital NHS Foundation Trust, London, UK.

[8] Institute of Metabolic Science, School of Clinical Medicine, University of Cambridge, Cambridge, UK.

[9] Department of Clinical Biochemistry, University of Cambridge, Cambridge, UK.

[10] Department of Comparative Biosciences, University of Illinois Urbana-Champaign, Urbana, IL, USA.

[11] Department of Bioengineering, University of Illinois Urbana-Champaign, Urbana, IL, USA.

[12] Cancer Center at Illinois, University of Illinois Urbana-Champaign, Urbana, IL, USA.

[*] Co-corresponding authors (eytan.ruppin@nih.gov, kwang222@illinois.edu)

ABSTRACT

The tumor microenvironment (TME) is a complex ecosystem of diverse cell types whose interactions govern tumor growth and clinical outcome. While multiple studies have extensively charted the TME's impact on immunotherapy, its role in chemotherapy response remains less explored. To address this, we developed DECODEM (DEcoupling Cell-type-specific Outcomes using DEconvolution and Machine learning), a generic computational framework leveraging cellular deconvolution of bulk transcriptomics to associate gene expression of individual cell types in the TME with clinical response. Employing DECODEM to analyze gene expression of breast cancer patients treated with neoadjuvant chemotherapy across three bulk cohorts, we find that the expression of specific immune cells (*myeloid*, *plasmablasts*, *B-cells*) and stromal cells (*endothelial*, *normal epithelial*, *CAFs*) are highly predictive of chemotherapy response, achieving the same prediction levels as the expression of malignant cells. Notably, ensemble models integrating the estimated expression of different cell types perform best and outperform models built on the original tumor bulk expression. These findings and the models' generalizability are further tested and validated in two single-cell (SC) cohorts of triple negative breast cancer. To investigate the possible role of immune cell-cell interactions (CCIs) in mediating chemotherapy response, we extended DECODEM to DECODEMi to identify such key functionally important CCIs, validated in SC data. Our findings highlight the importance of active pre-treatment immune infiltration for chemotherapy success. DECODEM and DECODEMi are made publicly available to facilitate studying the role of the TME in mediating response in a wide range of cancer indications and treatments.

INTRODUCTION

The tumor microenvironment (TME) is a complex and multifaceted ecosystem that encompasses a plethora of cell types including immune cells (such as T- and B-lymphocytes, macrophages, dendritic cells *etc.*), stromal cells (such as fibroblasts, endothelial cells *etc.*), and the extracellular matrix. It plays crucial roles in regulating tumor progression and response to therapy. Emerging evidence suggest context-specific behavior of the TME as either tumor-

59 suppressive or supportive, thus presenting an attractive target for therapeutic intervention
60 [1][2]. Numerous studies have elucidated the critical role of TME in mediating response to
61 immunotherapy, however, insights into how the TME is relevant to chemotherapy response
62 remains limited. Here we focus on studying the influence of the TME on chemotherapy
63 response in breast cancer (BC), where neoadjuvant chemotherapy (NAC) is used prior to
64 primary surgery to enable tumor downstaging and increase the likelihood of breast-conserving
65 surgery [3][4][5].
66
67 Recent studies have underscored the relevance of the BC TME in determining patient
68 response to chemotherapy. For instance, chemotherapy can induce dynamic changes in the
69 TME that lead to an increase in regulatory T-cells and myeloid-derived suppressor-like cells,
70 calling for a balance in immune population for positive treatment outcomes [6]. Lymphocyte
71 density and tumor infiltrating lymphocytes (TILs) have consistently been associated with BC
72 patients achieving pathological complete response (pCR) following NAC and anti-HER2 therapy
73 [7][8][9][10][11]. Additionally, multiple studies have reported the active involvement of TME in
74 therapy resistance [12][13][14], with macrophages, endothelial and BC stem cells promoting
75 chemoresistance [15][16][17], and B-cells and plasma cells displaying varying roles in NAC
76 response [18][19][20]. Based on this evidence, it is apparent that different cells within the TME
77 (and their interactions) contribute significantly to determining chemotherapy response.
78 However, to our knowledge, no study has yet attempted to quantify the contribution and
79 predictive power of each individual cell type within the TME to chemotherapy response in a
80 systematic and rigorous manner. We, therefore, aim to investigate three fundamental questions:
81 (1) Can we apply a rigorous computational approach to delineate the predictive power of cell-
82 type-specific transcriptome in the BC TME from bulk transcriptomics data? (2) Which cell types
83 in the BC TME and the corresponding pathways whose gene expression are most predictive of
84 chemotherapy response? (3) Does aggregating the inferred expression of multiple predictive cell
85 types in the BC TME lead to a more accurate clinical response predictor?
86

87 Current advances in precision oncology have highlighted the utility of artificial
88 intelligence [1][2][21][22][23][24] in guiding treatment using diverse data types such as
89 genomics [1][25][26], transcriptomics [29][30][31][32][33], histopathology
90 [34][35][36][37][38][39] or *via* multimodal approaches [11][27][28][40][41][42]. However,
91 investigations into neoadjuvant therapy response often encounter limitations such as small
92 sample size, treatment heterogeneity, or inadequate capturing of the TME's complexity, as
93 highlighted by Sammut et al. [11]. In their pioneering work, Sammut et al. presented a novel
94 multiomic predictor of neoadjuvant therapy response in BC [11]. They have leveraged machine
95 learning (ML) to incorporate 34 features extracted from clinical, DNA, RNA, pathology and
96 treatment data to develop a single model to predict patient response across all BC subtypes and
97 different treatment regimens with high accuracy. Expanding on this groundwork and addressing
98 the limitations, our study aims to decouple the cell-type-specific effects to NAC response in the
99 BC TME from transcriptomics alone by focusing on the HER2-negative (HER2-) patients, where
100 NAC is recommended to increase the likelihood of achieving pCR following surgery, especially in
101 triple negative breast cancer (TNBC) [43].
102
103 To systematically explore the association between the TME and chemotherapy response,
104 we developed a computational framework, **DECODEM** (DEcoupling Cell-type-specific Outcomes
105 using DEconvolution and Machine learning)**.** This framework leverages cellular deconvolution
106 with ML to elucidate the association of the expression of diverse cell types in the TME to patient
107 response to a given treatment. Recognizing that these phenotype effects are intricately
108 regulated by the interactions among relevant cell types within the TME, we further extended
109 DECODEM to **DECODEMi**, where 'i' stands for interaction. DECODEMi incorporates *inferred* cell-
110 cell interactions (CCIs) to pinpoint the key CCIs influencing treatment response. We
111 demonstrate the utility of our tools in an example scenario of investigating the role of the BC
112 TME in modulating NAC response across multiple bulk and single-cell (SC) cohorts,
113 demonstrating the markedly improved predictive capabilities of cell-type-specific transcriptome
114 over bulk and further pinpointing the notable CCIs. A recent study by Kester et al. investigated
115 the association of cellular compositions of the TME with patient survival in BC [44], but to our

knowledge, the current study is the first to analyze the *cell-type-specific transcriptomic profiles* in the BC TME to objectively quantify their association with treatment response. Together our findings point to the necessity of an active pre-treatment immune system to facilitate positive treatment outcome, as supported by Sammut et al. [11]. From a methodological perspective, our study provides tools to systematically assess the role of individual cellular components within the TME in anticancer therapy response (DECODEM) and to identify the prominent cell-to-cell communications associated with this response (DECODEMi).

RESULTS

Overview of the analysis

DECODEM and DECODEMi are new computational frameworks designed to explore the predictive powers of individual cell types and relevant cell-cell interactions, respectively, within the TME to response to therapy. They harness the prowess of CODEFACS and LIRICS, two recent tools from our laboratory [45]. CODEFACS facilitates the extraction of cell-type-specific expression profiles for each patient from their bulk gene expression, whereas LIRICS discerns the activity of cell-type-specific ligand-receptor interactions within their TME. In essence, DECODEM takes pre-treatment bulk gene expression data of a patient tumor sample as the input. It then uses deconvolution and machine learning to generate a score for each cell type indicating the likelihood that the patient will respond to the therapy. The predictive performance of these scores are quantified by using the standard classification metrics *i.e.*, area under the receiver operating characteristics curve (AUC), average precision (AP; equivalent to area under the precision-recall curve) and diagnostic odds ratio (DOR) metrics. DECODEMi then follows through to associate this response with CCIs in the TME to extract the most predictive interactions among these cell types.

Specifically, DECODEM comprises of two sequential steps (**Figure 1D**): *First*, for each bulk expression cohort, it generates nine cell-type-specific expression profiles for each sample across the whole transcriptome using CODEFACS with a BC-specific signature generated using scRNA-seq data (n = 26) from Wu et al. [46] (see **METHODS)** with annotations provided for nine major

145 cell types: *B-cells*, *cancer-associated fibroblasts (CAFs)*, *cancer epithelial (malignant)*,
146 *endothelial*, *myeloid*, *normal epithelial*, *plasmablasts*, *perivascular-like cells (PVL)* and *T-cells*;
147 *Second*, by leveraging these deconvolved expression profiles, it generates nine cell-type-specific
148 predictors of clinical response (classifying responders vs. non-responders *e.g.*, pCR vs. residual
149 disease) using a multi-stage ML pipeline. Within this pipeline, we performed rigorous feature
150 selection to keep the top '*m*' genes ($2 \leq m \leq 25$; the upper limit is chosen to avoid overfitting by
151 considering the confidently inferred genes) per cell type before feeding their expression into an
152 unweighted ensemble classifier consisting of four algorithms: regularized logistic regression,
153 random forest, support vector machine and XGBoost. The pipeline was trained with repeated
154 three-fold cross-validation (CV) to optimize model hyperparameters. Additionally, we built a
155 baseline predictor with bulk expression using the same ML pipeline to serve as a control,
156 comparative rod (we also built a second baseline predictor with the estimated cell fractions
157 that consistently underperformed the bulk baseline, thus opting to reporting only the latter).
158 Finally, as a sanity check, we performed a benchmark analysis for CODEFACS deconvolution
159 accuracy in breast cancer, our application domain. We used five BC benchmark cohorts where
160 patient pseudobulk samples were generated *via* mixing individual cells from Wu et al. [46] (see
161 **METHODS**). CODEFACS was then applied to these simulated bulk expression profiles with
162 known ground truth. The results reassuringly showed that CODEFACS achieved high accuracy
163 and successfully inferred thousands of genes accurately across cell types, thereby ensuring the
164 robustness of the deconvolution (**Supplementary Figure 1**).
165
166 To assess the performance of DECODEM and evaluate the contribution of each cell type,
167 we analyzed bulk transcriptomics data from three BC cohorts with different ratios of responders
168 to non-responders (R:NR) to NAC (**Figure 1A**) in two scenarios: (a) model development and
169 cross-validation with TransNEO (n = 94, R:NR = 22:72), recently published by Sammut et al. [11]
170 and (b) external validation on ARTemis + PBCP (n = 55, R:NR = 8:47) [47] and BrighTNess (n =
171 106, R:NR = 65:41) [48]. TransNEO and ARTemis + PBCP covered all major BC subtypes among
172 which we focused on the HER2- patients, treated with various chemotherapy regimens [11][47]
173 (**Figure 1A-B**), whereas BrighTNess included only TNBC patients from the arm B of the trial,

174 treated with paclitaxel and carboplatin with a placebo for veliparib [48]. We further validated
175 DECODEM's findings in two independent TNBC single-cell cohorts (**Figure 1C**): Zhang et al.,
176 which consisted of 15 patients receiving either paclitaxel alone (R:NR = 3:3) or in combination
177 with the anti-PD-L1 agent, atezolizumab (R:NR = 4:5) [49] and Bassez et al., which consisted of
178 six patients (R:NR = 3:3; taking T-cell clonotype expansion as a surrogate for patient response)
179 receiving a taxane – anthracycline based NAC before the anti-PD1 agent, pembrolizumab [50].
180 Notably, we took the Sammut et al. predictor built with 18 extracted features from clinical and
181 RNA-seq data (*e.g.*, not including the DNA-seq data) as a comparative rod that achieved an AUC
182 of 0.88 in CV and 0.89 in validation with ARTemis + PBCP [11], outperforming a baseline
183 predictor (AUC = 0.7) built with seven clinical features including ER and HER2 statuses, which
184 are routinely used to guide clinical decisions [43].
185
186 To investigate the impact of incorporating the expression profiles of multiple predictive
187 cell types together, as indicated by our third question, we applied two extensions to DECODEM:
188 (i) append the cell-type-specific expression profiles for two and three most predictive cell types
189 together to train a multi-cell-ensemble ML pipeline and (ii) extend to DECODEMi to incorporate
190 the inferred CCIs to train a CCI-based ML pipeline (**Figure 1D**). The former model maximizes the
191 predictive performance by leveraging complementary information from different cell types
192 while the latter identifies the most predictive cell-to-cell communications for clinical response,
193 thereby providing deeper insights to the underlying mechanism.
194

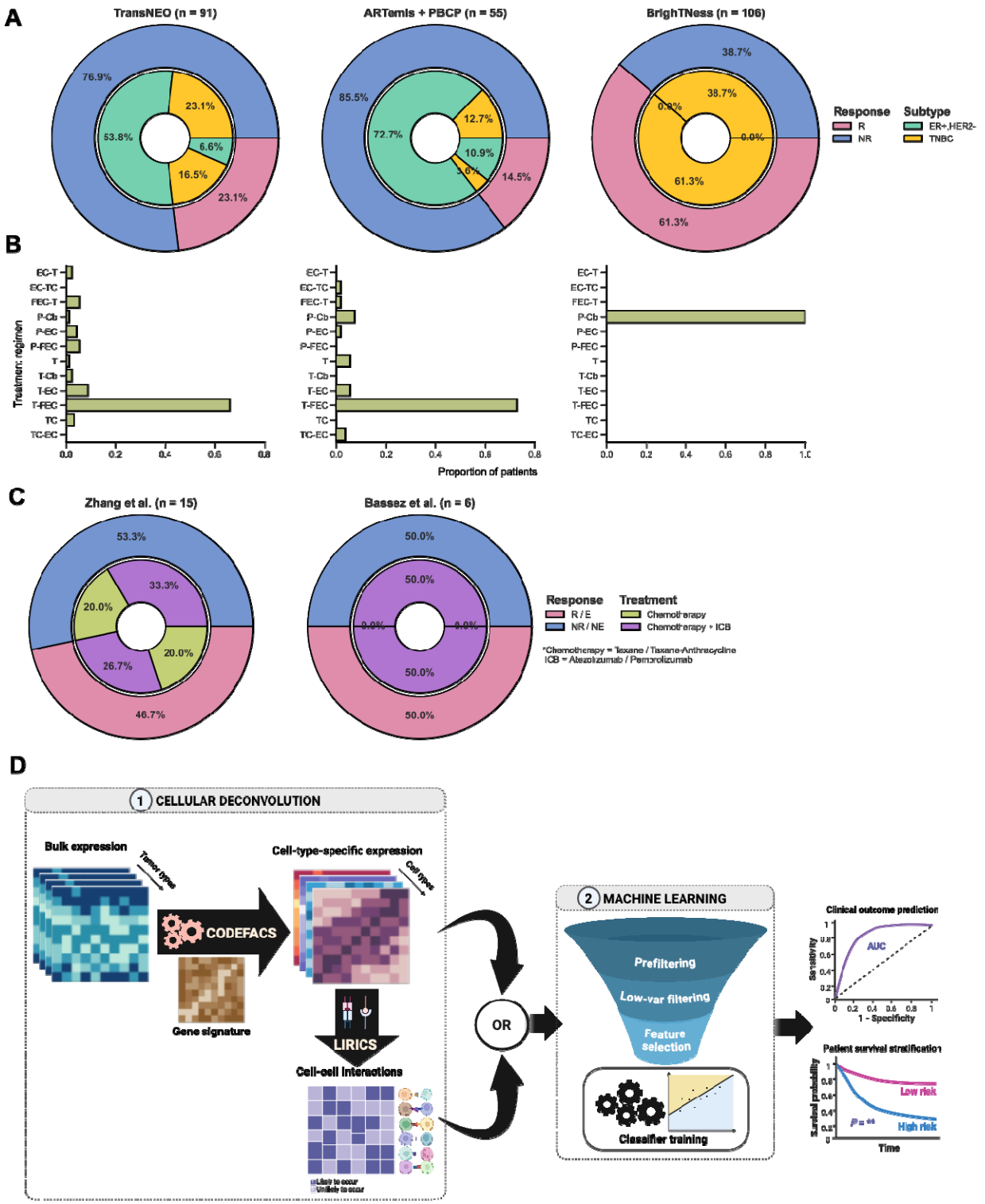

Figure 1: Overview of the methodology: cohorts and analysis.

A-B. Overview of the bulk cohorts used for analysis *i.e.*, the ratio of responders to non-responders (R:NR), clinical subtype distribution (**A**) and available treatment regimens (**B**) across

TransNEO, ARTemis + PBCP and BrighTNess. TransNEO was used for model development and the latter two were used for validation. ER+,HER2- and TNBC refer to the ER-positive, HER2-negative and triple negative breast cancer subtypes, respectively. *C*, *Cb*, *E*, *F*, *P* and *T* stand for cyclophosphamide, carboplatin, epirubicin, 5-flurouracil, paclitaxel and docetaxel (taxotere), respectively.

C. Overview of the single-cell (SC) TNBC cohorts used for external validation. The patients in Zhang et al. were analyzed separately based on treatment. For Bassez et al., T-cell clonotype expansion (E) and non-expansion (NE) was used as a surrogate for patient response. ICB stands for immune checkpoint blockade (anti-PD1 / anti-PD-L1) therapy.

D. The analysis pipeline, **DECODEM** and **DECODEMi**. *First*, we apply CODEFACS on bulk expression to infer cell-type-specific expression profiles or LIRICS for the cell-cell interactions (CCIs) present in the tumor microenvironment. *Second*, we train a multi-stage ML pipeline with these cell-type-specific expression profiles to build cell-type-specific clinical response predictors (DECODEM) or the binary CCI profile to build a CCI-based predictor (DECODEMi). For validation, we deploy the first stage above (bulk) or a customized pipeline (SC) to prepare cell-type-specific expression or CCIs and input to the trained predictors to evaluate model in terms of the area under the receiver operating characteristics curve (AUC) or stratify patient survival using Kaplan-Meier analysis.

Gene expression of immune and stromal cells predicts response to neoadjuvant chemotherapy as accurately as the expression of malignant cells

To assess the impact of individual cell types on chemotherapy response, we applied DECODEM to TransNEO in a CV analysis. Our analysis demonstrated significant differences (one-tailed Wilcoxon rank-sum test P-value ≤ 0.05) in the prediction scores between responders and non-responders across 91 patients (*i.e.*, patients with available prediction scores from Sammut et al.) in TransNEO (**Figure 2A**), with seven cell types exhibiting enhanced capabilities of identifying responders over the bulk and Sammut et al. predictors (**Figure 2D**). Notably, the immune cells (*myeloid*, *plasmablasts*, *B-cells*) contribute as prominently as malignant (*cancer epithelial*) and

228 stromal cells (*endothelial, normal epithelial, CAFs;* **Figure 2D**). Our subsequent analyses further
229 showed that these seven 'prominent' cell types accurately identify true responders to
230 chemotherapy with high average precision (**Figure 2G**) and diagnostic odds ratios (DOR; **Figure**
231 **2J**). We also investigated if training strategy impacts model performance by using a leave-one-
232 out CV instead of three-fold CV for hyperparameter tuning (maximizing accuracy) and obtained
233 similar performance (**Supplementary Figure 2**), supporting the robustness of our chosen
234 strategy.
235
236 These cell types have frequently been reported to influence clinical response in BC,
237 particularly in the context of chemotherapy-induced immunogenic cell death as the proposed
238 mechanism [52][11]. Changes in the immune population, such as an increase in regulatory T-
239 cells and myeloid-derived suppressor-like cells, and a decrease in $CD8^+$ T-cells, have been
240 associated with achieving pCR following NAC [6]. Myeloid cells have been implicated in therapy
241 response through interactions with the malignant and endothelial cells, inducing
242 chemoresistance *via* the *CXCL1/2 – S100A8/9* loop, whereas tumor-associated macrophages
243 have been linked to adverse outcomes and chemoresistance through survival factor secretion,
244 anti-apoptotic pathway activation and modulation of signaling pathways [6][15][16]. *VEGF*-
245 mediated upregulation of survivin in endothelial cells was further implicated in playing central
246 roles in chemoresistance [15]. Additionally, plasmablasts, as precursors of plasma cells, have
247 been associated with better prognosis [19][20], while B-cells have shown both pro- and anti-
248 tumor roles [18][19][20].
249
250 We further tested and validated the predictive power of these cell types in external
251 validation analyzing the ARTemis + PBCP (n = 55) and BrighTNess (n = 106) cohorts, observing
252 fairly consistent results (**Figure 2B-C, E-F, H-J**). The differences in score distributions across
253 cohorts (**Figure 2A-C**) likely stem from both biological variations due to cohort differences in
254 tumor subtypes, stages, tumor sample cell composition and ER / HER2 status, and variations
255 arising from out-of-distribution generalization effects (*e.g.*, different R:NR ratios across cohorts),
256 a well-known challenge in ML modeling. In the ARTemis + PBCP cohort (dominated by ER-

257 positive, HER2-negative (ER+,HER2-) BC), the prominent contributors to chemotherapy response
258 were CAFs, normal epithelial and malignant cells (**Figure 2E,H**), whereas in the TNBC-specific
259 BrighTNess cohort, the key players were myeloid, plasmablasts and malignant cells (**Figure 2F,I**).
260 For both cohorts, our prominent cell types accurately identified the responders with notably
261 high (>1.6) DOR values (**Figure 2J**) with variations observed across cohorts due to the effect of
262 cohort composition (*i.e.*, ARTemis + PBCP has few responders with R:NR = 8:47, as opposed to
263 BrighTNess with R:NR = 65:41). When stratifying TransNEO and ARTemis + PBCP cohorts by the
264 available BC subtypes, our cell-type-specific models retain good performance across subtypes
265 (**Supplementary Figure 3A-D**), although the models for ER+,HER2- BC were more predictive
266 than TNBC, possibly due to sample size limitations and the increased heterogeneity in TNBC.
267 These findings support the prominent involvement of immune and stromal cells with the
268 malignant cells in mediating patient response to chemotherapy within the TME, with variations
269 observed likely due to tumor subtype composition, stage and ER / HER2 status differences
270 across cohorts.
271

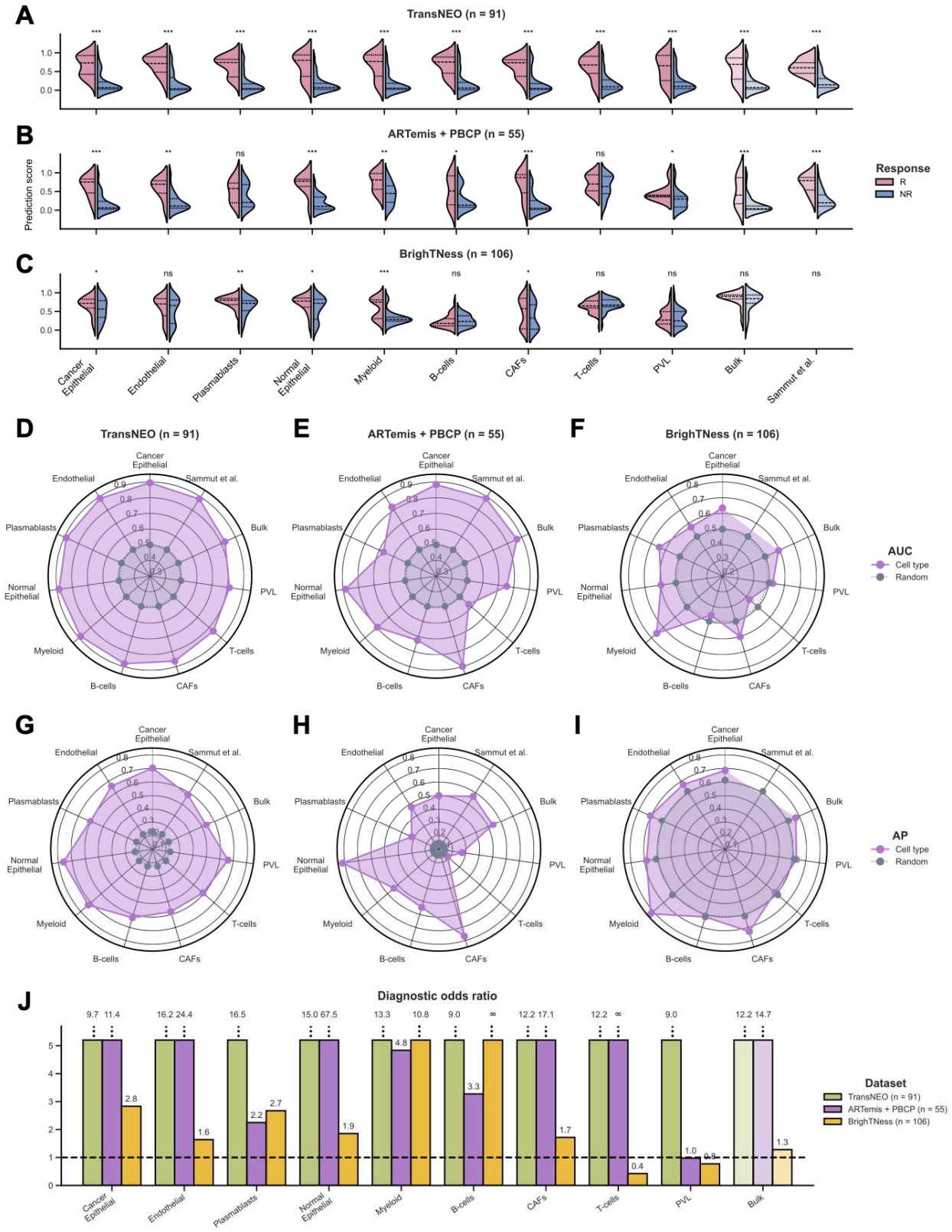
A
TransNEO (n = 91)
B
ARTemis + PBCP (n = 55)
C
BrighTNess (n = 106)
Prediction score
Response
R
NR
Cancer Epithelial
Endothelial
Plasmablasts
Normal Epithelial
Myeloid
B-cells
CAFs
T-cells
PVL
Bulk
Sammut et al.
D
TransNEO (n = 91)
E
ARTemis + PBCP (n = 55)
F
BrighTNess (n = 106)
AUC
Cell type
Random
G
H
I
AP
Cell type
Random
J
Diagnostic odds ratio
Dataset
TransNEO (n = 91)
ARTemis + PBCP (n = 55)
BrighTNess (n = 106)

273 **Figure 2: The prominent cell types mediating chemotherapy response in breast cancer tumor**
274 **microenvironment.**
275 **A-C.** Comparison of prediction scores for nine cell-type-specific, bulk and Sammut et al. (for
276 first two cohorts) predictors across TransNEO (**A**), ARTemis + PBCP (**B**) and BrighTNess (**C**). R and
277 NR stand for responders and non-responders, respectively. The differences between the
278 prediction scores were computed by using a one-tailed Wilcoxon rank-sum test (***, **, * and
279 'ns' denote $P \leq 0.001$, $P \leq 0.01$, $P \leq 0.05$ and $P > 0.05$, respectively). Cell types are ranked by
280 their AUC values for TransNEO in a descending order.
281 **D-I.** Comparison of model performance for nine cell-type-specific, bulk and Sammut et al. (for
282 first two cohorts) predictors across TransNEO (**D,G**), ARTemis + PBCP (**E,H**) and BrighTNess (**F,I**).
283 AUC and AP stand for the area under the receiver operating characteristics curve and average
284 precision, respectively. 'Random' denotes a random predictor (AUC = 0.5, AP = fraction of
285 responders). Cell types are ranked by their AUC values for TransNEO in a descending order in the
286 counterclockwise direction.
287 **J.** Comparison of diagnostic odds ratios (DOR) for nine cell-type-specific and bulk predictors
288 across the three cohorts. The dotted line represents a random predictor (DOR = 1.0). Cell types
289 are ranked by their AUC values in TransNEO a descending order.
290
291 Our analysis did not identify T-cells as a prominent predictive cell type, as their
292 expression provide marginal to no enhancement in predictive power over bulk expression
293 (**Figure 2D-J**). This lack of signal may stem from aggregating different T-cell subtypes together
294 (due to limits on the resolution of the deconvolution, which breaks down for low-abundance
295 cell types). To study this further, we performed an enrichment analysis to delineate the
296 contributions of $CD4^+$ and $CD8^+$ T-cells to chemotherapy response. However, the expression of
297 each of these cell types still exhibited limited stratification power to distinguish responders from
298 non-responders across the three bulk cohorts (**Supplementary Figure 4A-D**). We further
299 complemented this expression-based analysis with an association analysis of cell abundance
300 and clinical response, revealing that the overall T-cell abundance exhibited predictive power

similar to or even higher than $CD4^+$ and $CD8^+$ subtypes (**Supplementary Figure 4E-F**), albeit still notably lower than that of bulk.

An ensemble model incorporating the expression of immune and stromal cells significantly boosts the predictive power of patient response

To further enhance DECODEM's performance, we aggregated multiple individual cell types together by appending their expression profiles as input features. We explored 35 combinations of two to three cell types exhaustively, assessing whether a selective aggregation of multi-cell-type gene expression yields better predictive scores than the single-most predictive cell type. This comprehensive analysis achieved a boost in predictive performance for both ARTemis + PBCP and BrighTNess, with significant overlaps observed in top multi-cell-type ensembles across cohorts (**Figure 3A-F**). Remarkably, the ensemble of immune and stromal cells *i.e.*, the aggregation of the expressions of endothelial, myeloid and plasmablasts exhibited the strongest capability in identifying chemotherapy responders (*ARTemis + PBCP*: AUC = 0.94; *BrighTNess*: AUC = 0.75; **Figure 3D**). Additionally, the immune-cell-ensemble comprising myeloid and plasmablasts displayed high stratification (*ARTemis + PBCP*: AUC = 0.92; *BrighTNess*: AUC = 0.73; **Figure 3A**). As before, these multi-cell-ensembles also yielded high average precision (**Figure 3B,E**) and notably high (>5.0) DOR values (**Figure 3C,F**). These findings testify to the complementary contributions of diverse cell types within the TME to chemotherapy response. However, the top ensemble for BrighTNess provided a performance similar to the top cell type, myeloid (AUC = 0.76; **Figure 2F**), suggesting that the interactions among cell types are less prominent in this cohort compared to the others, expanded further in **Figure 4A-B**. The subtype-specific stratification of ARTemis + PBCP reinforced the superior predictive capabilities of these ensembles across two subtypes while recapitulating their diminished impact in TNBC (**Supplementary Figure 3E-F**).

We conducted gene set enrichment analysis (GSEA) with Reactome pathways [53] to explore the functional contributions of these prominent cell types in chemotherapy response

330 prediction. This analysis revealed the enrichment of cell cycle checkpoint and DNA replication
331 pathways across different cell types (false discovery rate (FDR)-adjusted *P*-value ≤ 0.2; **Figure**
332 **3G**) as the most common contribution. Dysregulation of these pathways are frequent in BC and
333 promotes tumor proliferation [54][55][56], making them valuable prognostic markers and
334 therapeutic targets [57][58][59][60]. Immune cells exhibited enrichment in signal transduction
335 pathways (*e.g.*, *VEGFA* – *VEGFR2* and *VEGF* signaling pathways in plasmablasts and multiple
336 *NOTCH1* signaling pathways in myeloid), implicated in malignant progression and therapy
337 resistance, particularly in TNBC [61][62][63][64][65][66][67]. Stromal endothelial cells showed
338 enrichment in development- and immune-related pathways (*e.g.*, *L1CAM* interactions and
339 antigen processing & presentation), contributing to aggressive BC progression and immune
340 evasion with implications for both chemo and immunotherapy [68][69][70][71][72][73][74].
341

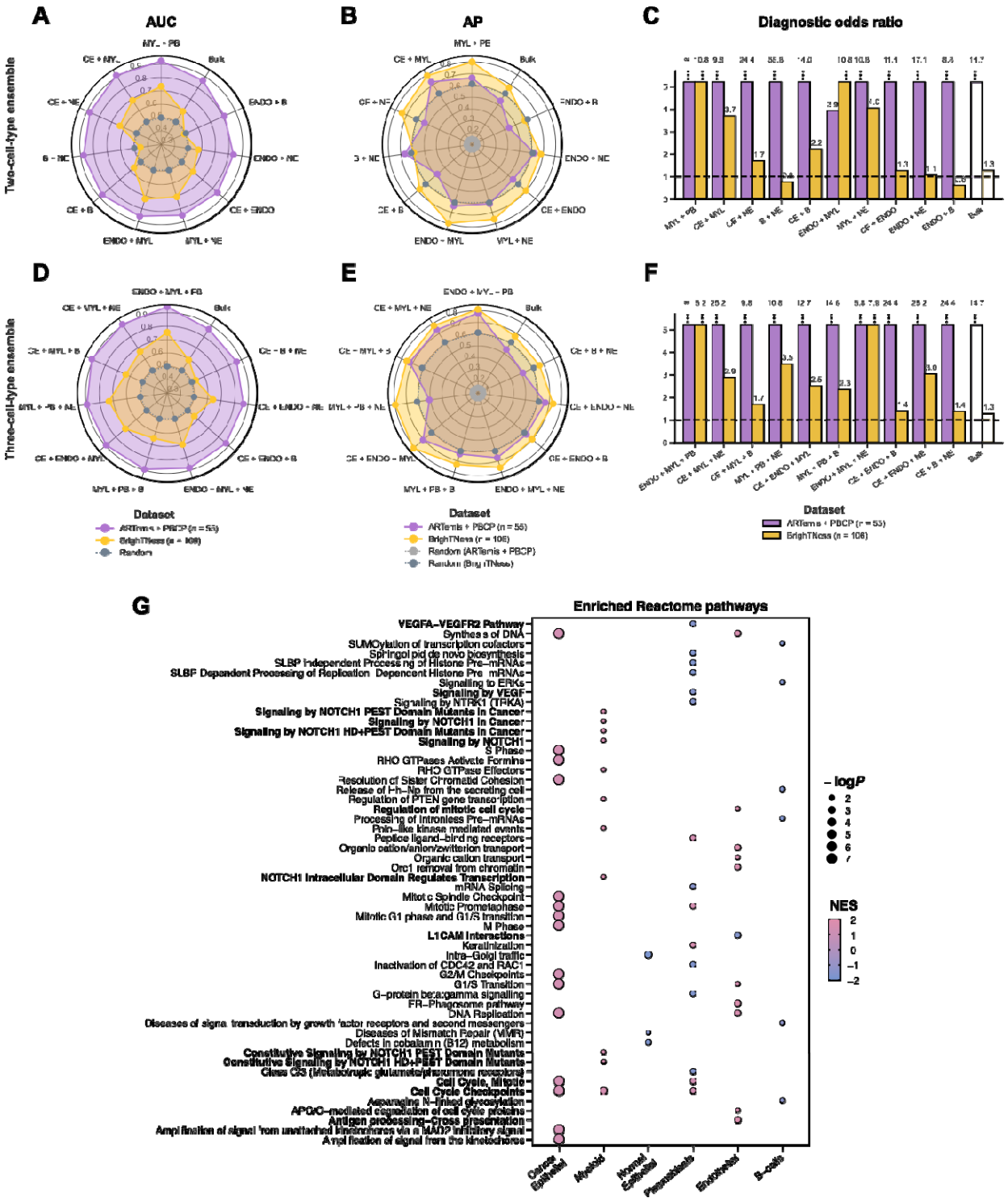

Figure 3: The prominent multi-cell-type ensembles mediating chemotherapy response in breast cancer tumor microenvironment.

345 **A-C.** Comparison of external validation model performance for the 10 most predictive
346 ensembles comprising of two cell types with the bulk predictor. *B*, *CE*, *ENDO*, *MYL*, *NE* and *PB*
347 stand for B-cells, cancer epithelial (malignant), endothelial, myeloid, normal epithelial and
348 plasmablasts, respectively. AUC and AP stand for the area under the receiver operating
349 characteristics curve and average precision, respectively. 'Random' denotes a random predictor
350 (AUC = 0.5, AP = fraction of responders). The dotted line in **C** represents the diagnostic odds
351 ratio (DOR) for a random predictor (DOR = 1.0). Ensembles are ranked by their mean AUC values
352 across cohorts in a descending order in the counterclockwise direction.
353 **D-F.** Comparison of external validation model performance for the 10 most predictive
354 ensembles comprising of three cell types with the bulk predictor. Ensembles are ranked by their
355 mean AUC values across cohorts in a descending order in the counterclockwise direction.
356 **G.** The significantly enriched Reactome pathways (FDR-adjusted $P \leq 0.2$) across six prominent
357 cell types. For each cell type, only the 10 most relevant pathways are displayed. NES and log*P*
358 stand for the normalized enrichment score from GSEA and log-scaled *P*-value, respectively.
359
360 We next assessed DECODEM's performance at a higher resolution considering the
361 prevalent chemotherapy regimen in each cohort. TransNEO and ARTemis + PBCP predominantly
362 employed T-FEC (n = 61 and 40, respectively; combining docetaxel (taxotere), 5-flurouracil,
363 epirubicin and cyclophosphamide), while BrighTNess used a regimen of paclitaxel and
364 carboplatin (**Figure 1B**). All six drugs display *immunogenic* effects by stimulating anticancer
365 immunity *via* either on-target (releasing immunostimulatory molecules from malignant cells) or
366 off-target (promoting activation of effector cells and diminishing immunosuppressive cells)
367 effects [74]. Remarkably, across all three cohorts spanning two BC subtypes and two treatment
368 regimens, DECODEM consistently identified myeloid, plasmablasts and B-cells to stratify
369 responders to immunogenic drug regimens, alongside the malignant cells (**Supplementary**
370 **Figure 5A-C**). For ARTemis + PBCP (dominated by ER+,HER2- BC), although the bulk mixture
371 displayed comparable or superior predictive power than each of these individual cell types,
372 their ensembles markedly boosted the performance, supporting the presence of prominent CCIs
373 involving these cell types that may be associated with the likelihood of response

(**Supplementary Figure 5D**). In addition, the ensemble of endothelial, myeloid and plasmablasts retains its highest performance, further underscoring the critical roles of stromal – immune interactions. For BrighTNess, the individual immune cell types showed notably strong predictive abilities, with less pronounced CCI effects (**Supplementary Figure 5E**, **Figure 4B-D**). Collectively, these findings corroborate the immunogenic cell death effects mediated by these chemotherapies [74], reinforcing previous suggestions by Sammut et al. [11].

Identifying key cell-cell interactions associated with chemotherapy response

To investigate the impact of the presence of interactions among different cell types in modulating chemotherapy response, we use DECODEMi to analyze CCIs (inferred using LIRICS [45], starting with 2,422 ligand – receptor (L-R) pairs from Ramilowski et al. [51]; see **METHODS**) that are predictive of patient response. As before, we conducted two analyses: (a) model development and cross-validation with TransNEO (n = 94) and (b) external validation on ARTemis + PBCP (n = 55) and BrighTNess (n = 106). As a preliminary analysis, we found that the CCIs encompassing the four most prominent cell types (*cancer epithelial*, *endothelial*, *myeloid* and *plasmablasts*) alone exhibited a classification power (one-tailed Wilcoxon rank-sum test P-value ≤ 0.05) comparable to all available CCIs across the three cohorts, further testifying to the influential roles of these prominent cell types in patient response (**Figure 4A-D**, **Supplementary Figure 6A-D**). The CCIs involving these four cell types markedly improved the predictive power of CCI-based predictors over bulk in both TransNEO and ARTemis + PBCP (**Figure 4B-D**). However, the CCI performance was generally lower than the top predictive myeloid cells in BrighTNess (**Figure 4B-D**), which can again be attributed to cohort composition, stage and treatment-specific variations. It is worth noting that BrighTNess included only later-stage TNBC patients treated with paclitaxel and carboplatin, a combination for which very few samples were available in training (**Figure 1A-B**). These results reinforced that leveraging information from multiple cell types can notably improve clinical response prediction and the intercellular crosstalk may be involved in mediating chemotherapy response within the TME.

403 To further assess the generalizability of DECODEMi, we evaluated its effectiveness on an
404 external single-cell TNBC cohort (SC-TNBC; sourced from Zhang et al. [48]). To overcome small
405 sample size limitation, we generated 200 'pseudopatients' treated with NAC (R:NR = 100:100)
406 by downsampling the 28,209 cells across the six TNBC patients from Zhang et al. who were
407 treated with paclitaxel [49]. Focusing on the CCIs involving the three cell types present in both
408 SC and deconvolved bulk data (B-cells, myeloid and T-cells), we identified the 170 most
409 predictive CCIs (covering 134 L-R pairs) from TransNEO and computed prediction scores for the
410 SC-TNBC cohort by aggregating the activated CCIs for each pseudopatient (as inferred by SOCIAL
411 [75]; see **METHODS**). Our analysis highlighted the significant predictive capabilities of these top
412 CCIs (one-tailed Wilcoxon rank-sum test *P*-value ≤ 0.001; AUC = 0.8; **Figure 4G-H**), affirming
413 DECODEMi's ability to identify the CCIs predictive of chemotherapy response from bulk
414 expression.
415
416 By computing feature importance from DECODEMi, we identified the most predictive
417 cell-to-cell communications across ARTemis + PBCP and BrighTNess, finding a significant overlap
418 in top CCIs (**Figure 4E-F**). Remarkably, the interaction between '*GDF9*' (growth differentiation
419 factor 9) and '*BMPR1B*' (bone morphogenetic protein receptor 1B), both members of the TGF-β
420 superfamily (the corresponding functional protein-protein interaction (PPI) network, obtained
421 from STRING [76], is provided in **Supplementary Figure 6E**) with roles in reproductive biology
422 and signal transduction [77][78][79][80], emerged as a key CCI with the same directionality
423 across multiple cell types. These genes have been implicated in BC prognosis and therapeutic
424 outcomes [81][82][83], with *BMPR1B* exhibiting dual roles in chemotherapy response
425 [84][85][86]. Another top CCI involved the renowned *GDNF – RET* signaling pathway interactions
426 between '*NRTN*' (neurturin) or its paralog '*ARTN*' (artemin) and '*GFRA1*' (GDNF family receptor
427 alpha 1) in multiple cell types (**Figure 4E-F**; see PPI network in **Supplementary Figure 6F**), which
428 are all members of the glial cell line-derived neurotrophic factor (GDNF) family within the TGF-β
429 superfamily with roles in neuronal survival, growth, and differentiation [87]. The GDNF family
430 exhibits diverse roles in cancer [88][89], including an association with therapy resistance in ER+
431 BC, highlighting *GFRA1* as a potential target [90][91][92][93]. Additionally, the well-studied

432 chemokine interaction between '*CX3CL1*' (C-X3-C chemokine ligand 1) and '*CX3CR1*' (C-X3-C
433 chemokine receptor 1) [94] is prominent in BrighTNess (**Figure 4F**; see PPI network in
434 **Supplementary Figure 6G**) and known to be involved in progression and metastasis across
435 multiple cancers including BC, presenting a promising pan-cancer target
436 [95][96][97][98][99][100].
437
438 Overall, DECODEMi application results in: (i) a simpler predictor leveraging CCIs that
439 improves patient stratification compared to bulk transcriptomics and (ii) the identification of
440 CCIs predictive of treatment response, whose activation is associated with pro-cancerous roles,
441 thus offering potential novel therapeutic targets.
442

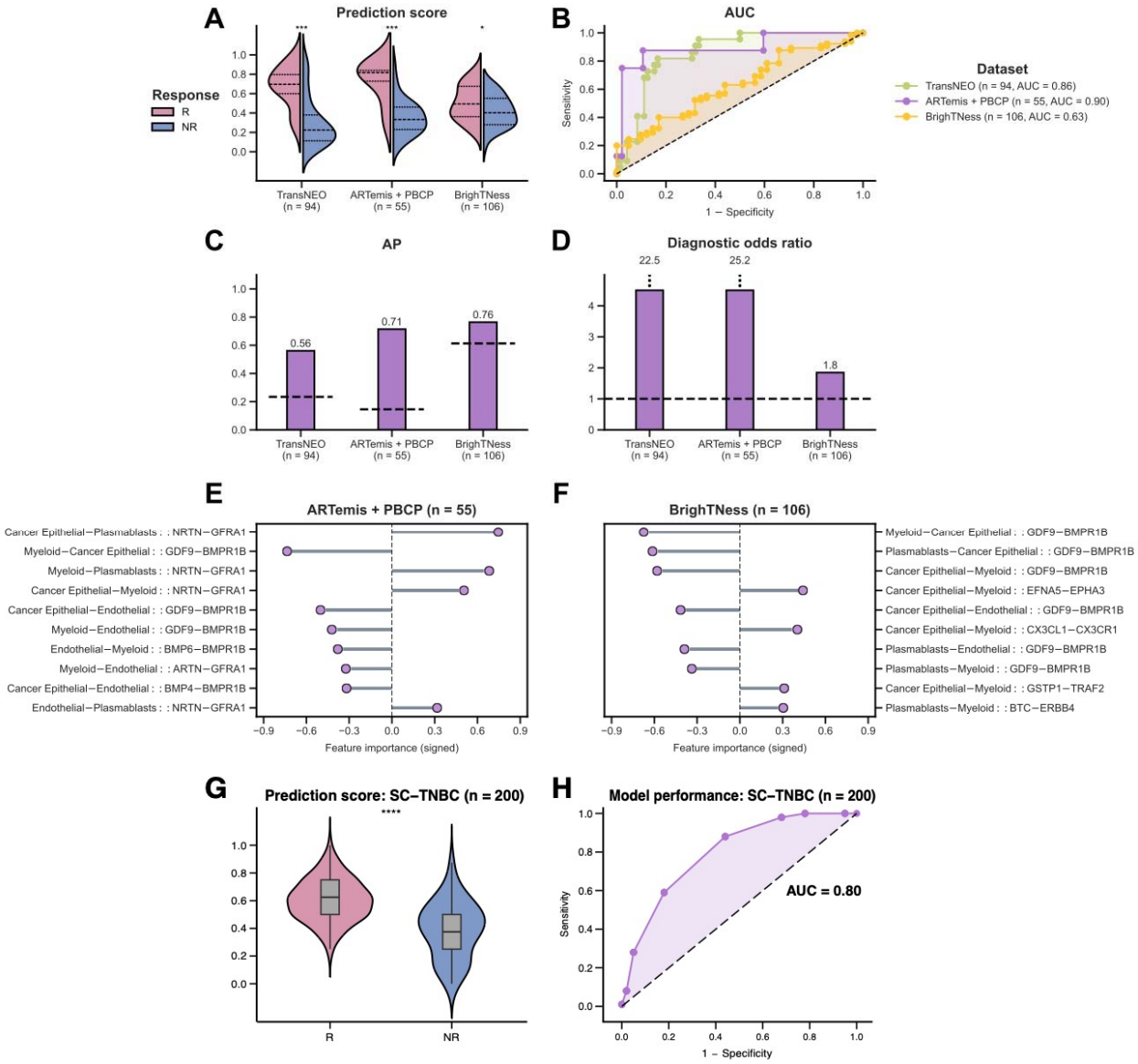

Figure 4: The prominent cell-cell interactions (CCIs) mediating chemotherapy response in breast cancer tumor microenvironment.

A-D. Comparison of prediction scores (**A**) and model performance (**B-D**) for DECODEMi CCI-based predictor across TransNEO, ARTemis + PBCP and BrighTNess. R and NR stand for responders and non-responders, respectively. The differences between the prediction scores were computed by using a one-tailed Wilcoxon rank-sum test (****, *** and * denote $P \leq 0.0001$, $P \leq 0.001$ and $P \leq 0.05$, respectively). AUC and AP stand for the area under the receiver operating characteristics curve and average precision, respectively. The dotted lines in **C-D**

452 represent the AP and diagnostic odds ratio (DOR) values for a random predictor (AP = fraction of
453 responders, DOR = 1.0).
454 **E-F.** The 10 most predictive CCIs in external validation with ARTemis + PBCP (**E**) and BrighTNess
455 (**F**). Each CCI is displayed as a quadruplet where the first pair containing the ligand and receptor
456 cell types (separated by '–') is separated by '::' from the second pair containing the
457 corresponding ligand and receptor genes (separated by '–'). Feature importance values were
458 computed by using Gini impurity (the built-in importance measure in random forest where a
459 higher value indicates a higher importance and *vice versa*). Feature directionalities were
460 computed by using a two-sided Fisher's enrichment analysis (*i.e.*, positive when odds ratio > 1
461 and *vice versa*).
462 **G-H.** Prediction scores (**G**) and model performance (**H**) in external validation with SC-TNBC (*n* =
463 200) using the top 170 response-relevant CCIs among B-cells, myeloid and T-cells, as identified
464 by DECODEMi in bulk.
465

466 DECODEM models predict patient response to chemotherapy and ICB 467 therapy as well as T-cell clonotype expansion from single-cell 468 transcriptomics

469 To further assess the generalizability of DECODEM, we evaluated the predictive capabilities of
470 the cell-type-specific models with single-cell transcriptomics. Due to the scarcity of publicly
471 available SC cohorts with NAC response, we extended our analysis to predict response to both
472 neoadjuvant chemotherapy and immune checkpoint blockade (ICB) therapy, shown to improve
473 pCR and approved recently as a first-line treatment in early-stage TNBC [101][102][103].
474
475 We first analyzed the Zhang et al. cohort [49] containing the expression of B-cells,
476 myeloid and T-cells for 15 TNBC patients, either treated with paclitaxel alone (*n* = 6) or
477 combined with the anti-PD-L1 agent, atezolizumab (*n* = 9). We stratified patients by treatment
478 and applied our established DECODEM models for these three cell types to predict response.
479 Notably, these models were trained on deconvolved TransNEO data without any further training
480 on SC data. Our findings revealed that for both intervention types, pre-treatment expression of

481 B-cells exhibited the highest responder stratification capability (one-tailed Wilcoxon rank-sum
482 test *P*-value ≤ 0.05; **Figure 5A**; **Supplementary Figure 7A-B**) and predictive potential (**Figure 5B**,
483 **Supplementary Figure 7D-E**). This is consistent with the findings from the original study that B-
484 cells at baseline display the highest association with favorable response to both chemotherapy
485 and ICB therapy [49]. Further, our analysis displayed a moderate predictive power for T-cells
486 (AUC: *chemotherapy* = 0.67; *chemotherapy + ICB* = 0.67; **Supplementary Figure 7D-E**), the major
487 hit from Zhang et al. [49], despite a weak T-cells-specific predictor (**Figure 2D-F**).
488
489 We next analyzed the Bassez et al. cohort [50] containing the expression of B-cells, CAFs,
490 malignant, endothelial, myeloid and T-cells for six TNBC patients, treated with chemotherapy
491 (taxane – anthracycline based) and the anti-PD1 agent, pembrolizumab. This study measured T-
492 cell clonotype expansion using scTCR-seq to identify patients with post-treatment clonotype
493 expansion vs. non-expansion (E vs. NE), which we take as a surrogate for response. Applying the
494 established cell-type-specific models, our analysis revealed myeloid, B-cells and endothelial as
495 the most predictive cell types at baseline (**Figure 5C-D, Supplementary Figure 7C,F**), consistent
496 with the original findings that certain pre-treatment macrophages are associated with T-cell
497 expansion while B-cells in tertiary lymphoid structures can impact ICB response [50]. Notably,
498 the study pointed to half of the NE patients having higher percentages of baseline T-cells (that
499 failed to expand post-ICB) [50], likely contributing to our finding of limited T-cells predictive
500 power.
501
502 These findings attest to the generalizability and robustness of DECODEM, highlighting its
503 potential in capturing the treatment-invariant properties of the BC TME to predict response to
504 the combination of chemotherapy and ICB therapy through SC transcriptomics.
505

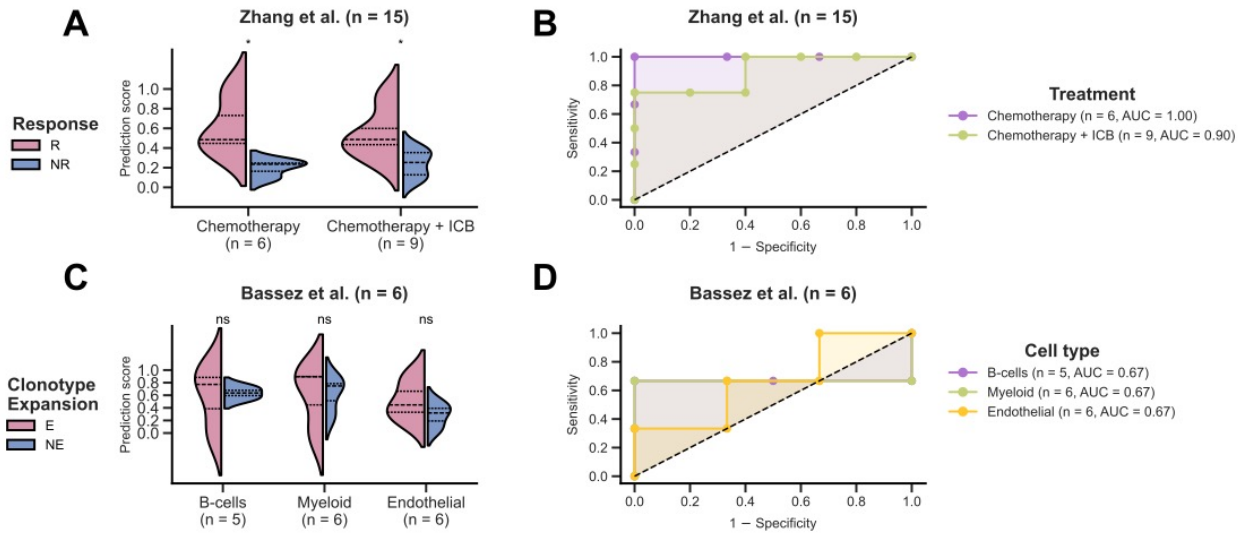

Figure 5: DECODEM generalizes to single-cell (SC) for clinical response prediction and for patient survival stratification.

A-B. Prediction scores (**A**) and model performance (**B**) for B-cells in external validation with Zhang et al. SC cohort for neoadjuvant chemotherapy and immune checkpoint blockade (ICB) therapy response prediction. T-cell clonotype expansion is taken as a surrogate for response in Bassez et al. R and NR stand for responders and non-responders, respectively. The differences between the prediction scores were computed by using a one-tailed Wilcoxon rank-sum test (* and 'ns' denote $P \leq 0.05$ and $P > 0.05$). AUC stands for the area under the receiver operating characteristics curve.

C-D. Prediction scores (**C**) and model performance (**D**) across cell types in external validation with Bassez et al. SC cohort for T-cell clonotype expansion prediction post-treatment with neoadjuvant chemotherapy and ICB. E and NE stand for expanders and non-expanders, respectively.

Similarly, we explored the prognostic capabilities of the DECODEM scores by using the early-stage HER2- breast cancer patients in TCGA-BRCA (n = 484) and achieved the most effective survival stratification across the malignant cells for both overall survival (**Supplementary Figure 8**) and progression-free interval (**Supplementary Figure 9**). These results

526 attest that the cell-type-specific models can indeed capture the treatment-invariant properties
527 of BC TME to indicate patient survival despite not explicitly training for it.
528

529 # DISCUSSION

530 Our study introduces DECODEM, a transcriptomics-based modeling framework harnessing
531 CODEFACS, a cutting-edge deconvolution tool, with a multi-stage machine learning pipeline to
532 systematically assess the cell-type-specific contributions to the prediction of clinical response to
533 treatment. As a representative scenario, we apply it to build predictors of patient response to
534 neoadjuvant chemotherapy in breast cancer. We further present DECODEMi, a companion tool
535 that identifies the key cell-cell interactions associated with such clinical response. A recent study
536 by Kester et al. investigated the association of cellular compositions of the BC TME with patient
537 survival [44], but to our knowledge, the current study is the first-of-its-kind to analyze the cell-
538 type-specific transcriptomics profiles in the BC TME to quantify their respective contributions to
539 treatment response prediction.
540

541 We applied DECODEM to investigate the predictive power of the expression of various
542 cell types in the BC TME to patient response to NAC. Our findings highlight the prominence of
543 immune cells (*myeloid*, *plasmablasts* and *B-cells*) in chemotherapy response, consistent with
544 Kester et al. [44], elucidating the complementary roles of diverse cell types that allows for the
545 incorporation of top predictive cell types to build accurate clinical response predictors, and
546 showcase DECODEMi's ability to identify key CCIs impacting response across HER2- BC.
547 Furthermore, we illustrated DECODEM's generalizability to SC transcriptomics capturing
548 treatment-invariant properties of the TME, thereby enabling accurate classification of
549 responders for chemotherapy and ICB. Moreover, we demonstrated DECODEMi's ability to
550 identify the top CCIs relevant to chemotherapy response and their generalizability to SC.
551

552 Immune cells have a clear association with prognosis in BC, both without and post
553 chemotherapy in the early-stage setting [107][30][31]. The International TILs Working Group
554 was established for the express purpose of standardizing incorporation of tumor infiltrating

555 lymphocyte pathological review for clinical use and established an online prognosis calculator
556 for patients with TNBC (https://www.tilsinbreastcancer.org/prognosis-tool/). Plasma cells and
557 naïve B-cells have been associated with better pCR rates in ER+ tumors, whereas regulatory T-
558 cells have been associated with better pCR rates in TNBC [108]. In our analysis, immune cells
559 such as plasmablasts and myeloid cells exhibit involvement in signal transduction, particularly
560 through *VEGF* and *NOTCH* signaling pathways, which are associated with tumor-associated
561 angiogenesis, enrichment of BC stem cells and epithelial-to-mesenchymal transition, thus
562 leading to poor prognosis and therapy resistance [61][62][65][67]. Stromal cells such as
563 endothelial cells display enrichments in development- and immune-related pathways including
564 *L1CAM* interactions and antigen processing and presentation, with *L1CAM*'s oncogenic role and
565 defects in antigen processing leading to poor outcomes and therapy resistance
566 [68][69][70][71][72]. Overall, our results paired with the existing clinical evidence reinforce that
567 the presence of an active immune infiltration within the TME prior to treatment, as indicated by
568 the prominent contribution of immune cells, leads to favorable chemotherapy response, as
569 suggested by Sammut et al. [11].
570
571 DECODEM and DECODEMi complement the existing application of gene expression in
572 the early-stage BC setting. Currently, gene expression-based tests such as Oncotype DX and
573 MammaPrint are used for prediction and prognostication in ER+ patients, reporting if a subset
574 should receive chemotherapy due to worse predicted outcomes [109]. These tests use
575 quantitative RT-PCR or cDNA microarray to assess a known subset of genes and largely apply
576 only to a subset of early-stage ER+ patients. DECODEM and DECODEMi provide complimentary
577 context to these tools, expanding applicable subtypes for chemotherapy response prediction
578 and the greater biological context.
579
580 Although we presented a comprehensive framework to assess the TME in a quantitative
581 manner, certain limitations should be acknowledged and addressed in future studies. *First*, our
582 predictors rely on data-driven algorithms involving deconvolution and ML, necessitating a large
583 sample size to attain statistical robustness and avoid overfitting. Accordingly, the available

584 cohorts are limited in size, limiting our ability to perform robust subtype-specific analyses.
585 *Second*, any limitations inherent to CODEFACS (*e.g.*, discrepancies in RNA-seq processing and
586 reliance on appropriate molecular signatures [45]) will affect DECODEM in downstream analysis.
587 Most of the cell types analyzed have well-defined gene signatures that allow for confident
588 deconvolution and downstream analysis. However, it is known to be more challenging to
589 distinguish between normal and cancer epithelial cells, which often employs copy number
590 variation (CNV) inference methods that are highly dependent on the correlation between
591 scRNA-seq and CNV along with the use of appropriate normal reference cells [110][111][112].
592 The same goes for DECODEMi and its reliance on LIRICS using an appropriate ligand – receptor
593 database [45]. *Third*, our deconvolution analysis could not be performed separately for $CD4^+$
594 and $CD8^+$ T-cell subsets. Alternatively, we provided an enrichment analysis assessing the
595 predictive powers of $CD4^+$ and $CD8^+$ T-cells that corroborated our findings from using the overall
596 T-cells.
597
598 Our work focused on examining the association of the BC TME, specifically in HER2- BC,
599 to clinical response to NAC. However, both DECODEM and DECODEMi can be applied to
600 investigate diverse treatment regimens (as shown with ICB) in different cancer indications.
601 Although both TransNEO and ARTemis + PBCP cohorts include different chemotherapy
602 combinations, limited sample size prevented us from exploring further. Therefore, an intriguing
603 direction could be to investigate the distinct role of the TME in different chemotherapy families
604 with different mechanisms of actions (MOAs) *e.g.*, taxanes, antimetabolites, platinum agents
605 and so on. With DECODEMi, one could further pinpoint the family-specific significant CCIs to
606 better elucidate the underlying MOA and uncover novel CCIs with promising therapeutic
607 implications. Additionally, expanding the investigation beyond the scope of cancer and
608 examining the impact of the microenvironment in various indications such as aging-related
609 disorders and autoimmune diseases could provide further valuable insights.
610
611 In summary, our study introduces two data-driven computational frameworks that
612 enable systematic investigation of the roles of the microenvironment in various processes,

including treatment response. These frameworks can utilize bulk transcriptomics from healthy and diseased conditions when single-cell information is not easily accessible, providing a valuable approach to study the TME in a comprehensive manner. Their application in breast cancer uncovers the considerable predictive power of diverse cell types within the TME and highlights key stromal – immune CCIs that are strongly predictive of patient response. Taken together, we show that ensemble models integrating the expression of different cell types perform best and outperform models built on the original tumor bulk expression.

METHODS

Overview of the cohorts

We analyzed three bulk transcriptomics cohorts, encompassing a total of 255 breast cancer patients who received neoadjuvant chemotherapy (**Figure 1A-B**). The first cohort, recently published by Sammut et al., was the TransNEO cohort which included 94 HER2- breast tumors from patients undergoing various NAC regimens (**Figure 1B**) [11]. Notably, Sammut et al. presented the complete TransNEO cohort, covering 168 patients with early and locally advanced BC from all major subtypes, and provided DNA-seq, RNA-seq, digital pathology and treatment information for various subsets of patients [11]. The second cohort was the ARTemis + PBCP cohort, externally validated by Sammut et al., combining the control arm of the ARTemis trial (*n* = 38) received the combination therapy of FEC-T [47] and the HER2- cases from the Personalised Breast Cancer Programme (PBCP; *n* = 17) undergoing various NAC regimens [11] (**Figure 1B**). The third cohort, BrighTNess, included 106 patients from arm B of the BrighTNess trial, a randomized, double-blind, placebo-controlled three-arm clinical study for veliparib in stage II/III TNBC [48]. Arm B included only patients who received the NAC combination of paclitaxel, carboplatin, and a placebo for veliparib (**Figure 1B**). In all three cohorts, patient response was assessed at surgery using the residual cancer burden (RCB) index where patients achieving pathological complete response (pCR; RCB = 0) were taken as responders (R) and patients with residual diseases (RCB-I, II, III) as non-responders (NR) with different R:NR ratios (**Figure 1A**).

641 Furthermore, we analyzed two recent single-cell cohorts encompassing 21 patients with
642 triple negative breast cancer, treated either with chemotherapy alone (*n* = 6) or chemotherapy
643 and immune checkpoint blockade therapy (*n* = 15; **Figure 1C**). The first SC cohort was presented
644 by Zhang et al. that consisted of 15 patients with pre-treatment tumor biopsy expression of four
645 immune cell types (B-cells, innate lymphoid cells, myeloid and T-cells) and either treated with
646 paclitaxel alone (*n* = 6) or combined with the anti-PD-L1 agent, atezolizumab (*n* = 9) [49].
647 Notably, this study originally comprised of 22 patients with advanced TNBC, where only half of
648 the patients received combination therapy [49], and included 78 tumor biopsies and blood
649 samples collected at three time-points including baseline. The patient response at surgery were
650 assessed using the Response Evaluation Criteria in Solid Tumors (RECIST) criteria [49], where we
651 categorized patients achieving complete or partial response as responders (R) and those with
652 stable or progressive diseases as non-responders (NR). We divide Zhang et al. into two sub-
653 cohorts for analysis based on treatment *i.e.*, chemotherapy (*n* = 6) and chemotherapy + ICB (*n* =
654 9; **Figure 1C**). The second SC cohort was presented by Bassez et al. that consisted of 6 TNBC
655 patients with pre-treatment tumor biopsy expression of six cell types (B-cells, CAFs, endothelial,
656 malignant, myeloid and T-cells) and treated with taxane – anthracycline based neoadjuvant
657 chemotherapy before receiving the anti-PD1 agent, pembrolizumab [50] (**Figure 1C**). This cohort
658 was part of the window-of-opportunity study, BioKey, involving early diagnosed BC (including all
659 major subtypes) that included one cohort of 29 treatment-naïve patients and another cohort of
660 11 patients treated with neoadjuvant chemotherapy (and anti-HER2 therapy for HER2+
661 patients) for 20-24 weeks, both followed by pembrolizumab before surgery. This study collected
662 tumor biopsies at both pre- and on-treatment and performed scRNA-seq and scTCR-seq on the
663 same SC suspension using 10x sequencing technologies [50]. As patient response were not
664 available, we considered the post-treatment T-cell clonotype expansion assessed from scTCR-
665 seq data as a surrogate variable while only considering the TNBC patients from the second
666 cohort (*n* = 6), since they were treated with NAC and ICB therapy and included both clonotype
667 expanders and non-expanders (E:NE = 3:3; unlike the 4 ER+ patients who displayed NE only)
668 [50].
669

Deconvolution with CODEFACS

The first step of DECODEM involves employing CODEFACS, a cellular deconvolution tool recently developed in our laboratory [45] (**Figure 1D**). CODEFACS characterizes the TME by reconstructing the cell-type-specific expression across the whole transcriptome in each sample from input bulk expression by utilizing the corresponding cell abundance or a cell-type-specific signature matrix as another input. The output includes the cell-type-specific expression profiles, cell abundance and a confidence score matrix quantifying the confidence level (between 0 and 1) of the inferred expression values for each gene in each cell type across all samples.

As a sanity check. we first tested the ability of CODEFACS to accurately deconvolve bulk expression profile into different cell-type-specific expression profiles for breast cancer samples. We leveraged a SC cohort recently presented by Wu et al. [46] that contained 26 primary breast tumors (11 ER+, 5 HER2+ and 10 TNBC) encompassing 130,246 single cells across nine major cell types and generated five benchmark cohorts (BC1 – BC5) following the benchmark generation procedure in Wang et al. [45]. BC1 contains pseudobulk expression for deconvolution and the corresponding ground truth data (cell abundance and cell-type-specific expression) for 22 out of 26 original patients (keeping 4 patients aside for signature generation with CIBERSORTx [105]); BC2 and BC3 contain 100 'pseudopatients' each with different mixtures of cells; and BC4 and BC5 denote two noisy versions of BC1. Using CODEFACS, we inferred nine different cell types from each cohort and evaluated deconvolution accuracy by measuring the Kendall correlation (τ) between the observed and inferred values following Wang et al. [45], yielding high accuracy for both the cell-type abundance (**Supplementary Figure 1A**) and cell-type-specific expression (**Supplementary Figure 1B**). We also quantified thousands of accurately inferred genes ($\tau \geq 0.3$, $P \leq 0.05$) on average across cell types (**Supplementary Figure 1C**).

We then used this scRNA-seq data (with original cell type annotation) from Wu et al. to derive a breast cancer-specific cell type signature matrix encompassing 1,400 genes representing the nine cell types using an in-house signature derivation tool based on CIBERSORTx [105]. We employed this signature matrix to deconvolve each bulk expression

profile into nine cell-type-specific expression profiles across the unique protein-coding genes available per cohort (TransNEO = 17,680, ARTemis + PBCP = 17,940 and BrighTNess = 15,203). The aforementioned nine cell types were: *B-cells*, *cancer-associated fibroblasts (CAFs)*, *cancer epithelial (malignant)*, *endothelial*, *myeloid*, *normal epithelial*, *plasmablasts*, *perivascular-like cells (PVL)* and *T-cells*.

Curation of a database of cell-type-specific ligand – receptor interactions in BC TME from single-cell

To infer the cell-cell interaction activity using LIRICS, we first constructed a database of cell-type-specific ligand – receptor interactions (LRIs) to characterize all cell-to-cell communications that are likely to occur within the TME of BC patients. To this end, we obtained a list of 2,422 potential L-R pairs annotated by Ramilowski et al. [51] and evaluated the potential of each pair occurring between the nine cell types of interest using the scRNA-seq data from Wu et al. again [46]. To discern the activity of the curated L-R pairs between cell types, we pooled together all 130,246 cells from Wu et al. and applied an empirical *P*-value based CCI inference approach using SOCIAL from Sahni et al. [75] (with a modified assumption of true LRI activity < null LRI activity in step 3), where an LRI with $P \leq 0.05$ was categorized as 'likely' to occur in BC TME and 'unlikely' otherwise, following the standard practices in the field. This procedure enabled us to construct a database of 49,397 cell-type-specific L-R pairs (*i.e.*, CCI quadruplets including ligand cell type, ligand gene, receptor cell type and receptor gene) that are likely to occur in the BC TME. This database composed the initial feature space for LIRICS to yield different numbers of CCIs across the three bulk cohorts (*i.e.*, TransNEO = 46,755, ARTemis + PBCP = 43,887 and BrighTNess = 38,285).

Extraction of cell-cell interactions with LIRICS

We extended DECODEM to DECODEMi by incorporating multi-cell-type information through CCIs (**Figure 1D**). To this end, DECODEMi applies LIRICS [45] on the output of CODEFACS to infer the corresponding CCI activity. LIRICS uses a two-step approach on deconvolved expression to infer the cell-type-specific ligand – receptor (L-R) pairs that are likely to be 'active' in each

sample: *First*, it queries a database of 49,397 plausible L-R interactions between each pair of cell types in the BC TME, constructed using SC data (see above); *Second*, it then infers an L-R interaction as active in a pair of cell types in a given sample (indicated by '1') if the expressions of both ligand and receptor genes exceed their median cell-type-specific expression values or inactive otherwise (indicated by '0') [45]. We used this binary CCI activity matrix from LIRICS to assess the predictive potential of cell-to-cell communications.

Machine learning pipeline with deconvolution output

The second step of both DECODEM and DECODEMi involves building ML predictors of clinical response using either cell-type-specific expression profiles or CCIs, respectively. For DECODEM, we built nine cell-type-specific predictors to classify R vs. NR following treatment using a four-stage ML pipeline (**Figure 1D**): (a) unsupervised prefiltering to keep only the genes that are deconvolved with a confidence score ≥ 0.99, (b) low-variance filtering to keep genes with variance ≥ 0.1, (c) supervised feature selection to select the top 'm' genes maximizing performance, where $2 \leq m \leq 25$ with genes ranked by their ANOVA F-scores for association with response, followed by standardization to scale each gene to zero mean and unit variance, and (d) classification with an unweighted ensemble classifier comprised of regularized logistic regression, random forest, support vector machine and XGBoost (extreme gradient boosting) to predict the likelihood scores of response. The upper limit on the feature size is chosen to avoid model overfitting (by ensuring a lower feature size than sample size), reduce noise and facilitate shorter runtimes. Of note, we tested different feature sizes (m = 25, 50, 100) that yielded similar performance during model development and hence opted for the smallest size to ensure greater robustness. Furthermore, each score vector was rescaled between 0 and 1 across samples to improve out-of-distribution generalization. We trained the pipeline using three-fold cross-validation (CV) for hyperparameter tuning to maximize the area under the receiver operating characteristics (ROC) curve (AUC) for each classifier separately. To avoid overfitting, we repeated the training procedure five times with five different CV splits and took the mean of the five prediction vectors as our final prediction. Moreover, we investigated model performance by replacing the CV with a leave-one-out CV for hyperparameter tuning

757 (maximizing accuracy) and obtained similar performance (**Supplementary Figure 2**), thereby
758 opting to use the three-fold CV for main analyses. Once trained, we applied the test data to the
759 trained models to yield model predictions and evaluate their performance using one-tailed
760 Wilcoxon rank-sum test (*P*-value ≤ 0.05), ROC curve and precision-recall (PR) curve analysis. We
761 further evaluate performance by computing the clinically relevant measure of diagnostic odds
762 ratio (DOR), where we binarized the prediction scores using an optimal threshold learned from
763 optimizing the training PR curve.
764
765 To accommodate for the sparse nature of SC transcriptomics (and CCI profile) for
766 external validation, we slightly modified the pipeline to enable modeling for all available genes
767 post filtering in step (c) *i.e.*, $2 \leq m \leq$ 'all'. Furthermore, to align SC expression with CODEFACS
768 output (which provides the mean cell-type-specific expression profile per patient [45]), we
769 harmonized the cell-type-specific SC expression by averaging across all corresponding cells for
770 each patient, while only taking the top 3,500 highly variable genes to reduce noise. Additionally,
771 for CCI-based analysis with DECODEMi, we skipped step (a) and further updated the low-
772 variance cut-off in step (b) to 0.08 and the classifier in step (d) to random forest that is better
773 suited to the binary nature of input CCI matrix and includes a built-in measure of feature
774 importance, mean decrease in Gini impurity. For signed feature importance, the CCI
775 directionalities were computed by using a two-tailed Fisher's test (followed by false discovery
776 rate (FDR) adjustment for multiple hypothesis correction *i.e.*, FDR-adjusted *P*-value ≤ 0.05),
777 where an odds ratio (OR) > 1 denotes an enrichment in responders and *vice versa*. Moreover,
778 for filtering CCIs for the prominent cell types, we only include the interactions involving the
779 confident L-R genes (CODEFACS confidence level ≥ 0.99) in the corresponding cell type.
780
781 For baseline comparison in DECODEM, we employed the same ML pipeline while
782 skipping the prefiltering in step (a) for training with bulk transcriptomics (and further skipping
783 feature selection in step (c) for training with cell abundance). For DECODEMi, we calculated the
784 overall 'pseudobulk' expression (akin to the bulk mixture) as the mean expression across all cells
785 covering all available cell types for each patient in a cohort post low-variance filtering (as

786 described above). Additionally, since our framework dynamically adapts to the feature size
787 available in both training and validation, we provide a validation script that generates the cell-
788 type-specific and CCI-based models for a new validation cohort, essentially providing a 'cohort-
789 specific locked-down model'.
790

791 $CD4^+$ / $CD8^+$ T-cells enrichment analysis

792 To analyze the contribution of the individual T-cell subtypes to chemotherapy response, we
793 performed a gene set variation analysis (GSVA) to summarize the pathway activities per sample
794 for each T-cell subtype. We employed two SC expression signatures derived from Wu et al. [46],
795 collected *via* the Tumor Immune Single Cell Hub 2 (TISCH2) [106] and performed GSVA on the
796 deconvolved T-cells expression using the GSVA R package. These signatures consisted of 207
797 and 424 differentially expressed genes (DEGs) for $CD4^+$ and $CD8^+$ T-cells, respectively, with log-
798 fold-change ≥ 0.5 and an overlap of 151 DEGs. Subsequently, we evaluated the association of
799 GSVA enrichment scores (rescaled between 0 and 1) with clinical response across the three bulk
800 cohorts using a one-tailed Wilcoxon rank-sum test (FDR-adjusted *P*-value ≤ 0.05; **Supplementary**
801 **Figure 4A,C**), ROC and precision-recall curve analyses (**Supplementary Figure 4B,D**).
802

803 Cell-type-specific enrichment analysis

804 We conducted gene set enrichment analysis (GSEA) to investigate the association of each cell
805 type with different biological processes. For each cell type, we first ranked the 17,680 protein-
806 coding genes available in TransNEO by their association with positive outcome (*i.e.*, pCR),
807 measured by the *P*-values from a one-tailed Wilcoxon rank-sum test, adjusted by CODEFACS
808 confidence scores. We performed a separate GSEA analysis using the Reactome pathways [53]
809 for each prominent cell type (except CAFs), yielding six different sets of enriched pathways
810 (FDR-adjusted *P*-value ≤ 0.2) across six prominent cell types. From these sets, we reported the
811 top 10 relevant pathways for each cell type (**Figure 3G**).
812

Single-cell validation of top CCIs from bulk

We validated the most predictive CCIs extracted by DECODEMi in bulk using a validation cohort sourced from the pre-treatment SC expression of six TNBC patients from Zhang et al., who were treated with NAC [49]. We devised a three-step validation procedure: *First,* for consistency, we retrained DECODEMi with TransNEO including only the interactions among cell types available in both bulk and SC (*B-cells*, *myeloid* and *T-cells*). This enabled us to extract the top predictive CCIs (m = 170) involving a total of 134 unique L-R pairs. *Second*, to enhance the statistical power and robustness, we pooled the 28,209 cells encompassing the three cell types across all six patients and randomly downsampled 30% cells 100 times within each response group for each cell type. This procedure generated a profile of 200 pseudopatients (R:NR = 100:100) with empirical *P*-values denoting the significance levels of the 804 possible CCIs involving the 134 L-R pairs in three cell types (= 134 × 2 × 3), yielding the 'SC-TNBC cohort'. To identify the activation status of these 170 CCIs of interest within this cohort, we applied the SOCIAL-based CCI inference approach [75] described above to denote a CCI status as 'active' if $P \leq 0.05$ and 'inactive' otherwise. *Third*, for each pseudopatient, we predicted chemotherapy response as the sum of active CCIs, signed by their directionalities (*i.e.*, + or - when OR > 1 or < 1, FDR-adjusted *P*-value ≤ 0.05; and 0 otherwise), followed by a rescaling between 0 and 1 across all pesudopatients. We then used these prediction scores to validate the performance of these top CCIs using a one-tailed Wilcoxon rank-sum test (FDR-adjusted *P*-value ≤ 0.05) and ROC curve analysis (**Figure 4G-H**).

Patient survival stratification in TCGA-BRCA

We explored whether the DECODEM scores can be used to stratify the survival of the 484 early-stage HER2- breast cancer patients (encompassing stages I – IIIA following the training cohort, TransNEO, that included early-stage BC patients only) in The Cancer Genome Atlas (TCGA-BRCA) from their cell-type-specific expression. Focusing on the expression of the prominent cell type of malignant cells (top performer across subtypes; **Supplementary Figure 3**), DECODEM effectively stratified the patients within each BC subtype into High-score and Low-score groups (implying low- and high-risk, respectively) using a fixed threshold of 0.5, as displayed by their

Kaplan-Meier curves for overall survival (Log-rank test *P*-value ≤ 0.05, **Supplementary Figure 8A-B**) and progression-free interval (**Supplementary Figure 9A-B**). The remaining prominent cell types also displayed similar survival trends (**Supplementary Figure 8C-N, Supplementary Figure 9C-N**).

DATA AVAILABILITY

For TransNEO cohort, RNA-seq counts and clinical data were acquired from the publication by Sammut et al. (https://doi.org/10.1038/s41586-021-04278-5). RNA-seq counts were converted to TPM by using Ensembl annotations (GRCh37.87, http://ftp.ensembl.org/pub/grch37/release-87/gtf/homo_sapiens/). For ARTemis + PBCP cohort, clinical data were collected from Sammut et al. (https://doi.org/10.1038/s41586-021-04278-5) and RNA-seq TPM values were obtained from the authors. For BrighTNess cohort, RNA-seq FPKM values (converted to TPM) and clinical data were acquired from the gene expression omnibus (GEO; accession no: GSE164458; https://www.ncbi.nlm.nih.gov/geo/query/acc.cgi?acc=GSE164458). For Zhang et al., scRNA-seq counts and clinical data were obtained from the publication itself (https://doi.org/10.1016/j.ccell.2021.09.010). For Bassez et al., scRNA-seq counts and clinical data were obtained from Lambrechts Lab website (https://lambrechtslab.sites.vib.be/en/single-cell). For Wu et al., scRNA-seq counts and cell annotations were collected from GEO (accession no: GSE176078; https://www.ncbi.nlm.nih.gov/geo/query/acc.cgi?acc=GSE176078) and the list of differentially expressed genes across cell types were collected from TISCH2 (http://tisch.comp-genomics.org/gallery/). The ligand-receptor list from Ramilowski et al. were collected *via* GitHub (https://github.com/LewisLabUCSD/Ligand-Receptor-Pairs). For TCGA-BRCA, RNA-seq counts (converted to TPM), survival data and clinical data were collected from the UCSC Xena browser (https://xenabrowser.net). All deconvolved expression and cell-cell interaction data generated in this study will be made available upon publication.

CODE AVAILABILITY

All relevant codes for reproducing the figures in this study are publicly available upon publication at https://github.com/ruppinlab/DECODEM/. The codes for CODEFACS and LIRICS

are available from the original publication at https://zenodo.org/record/5790343/. The codes for molecular signature generation are available at https://github.com/ruppinlab/scSigR/.

ACKNOWLEDGEMENTS

This research is supported in part by the Intramural Research Program of the National Institutes of Health, National Cancer Institute, Center for Cancer Research. This work has utilized the computational resources of the NIH HPC Biowulf cluster (http://hpc.nih.gov). The results presented are in part based on the data generated by The Cancer Genome Atlas Research network (https://www.cancer.gov/tcga/). We would additionally like to acknowledge Thomas Cantore for helpful discussion regarding cellular deconvolution and survival analysis, Sanna Madan and Danh-Tai Hoang for guidance pertaining cell type identification and data visualization, E. Michael Gertz for data collection and helpful discussion regarding survival analysis, and the members of the Cancer Data Science Laboratory for their constructive feedback. Panel D in Figure 1 has been created in BioRender (Dhruba, S. R. (2025) https://BioRender.com/z38y774). ChatGPT v4o (https://chatgpt.com/) was used strictly to refine certain existing paragraphs for better overall presentation.

AUTHOR CONTRIBUTIONS

S.R.D, K.W. and E.R. conceived and designed the study. S.R.D., S.S. and K.W. performed the model development and validation analyses. S.R.D., K.W., S.S., P.S.R., B.W., Y.S., E.S., S.Si., S-J.S., C.C. and E.R. acquired, analyzed or interpreted the data. S.R.D., S.S., K.W., D.W., S.Si. and B.W. worked on data visualization. E.R. and K.W. supervised the study. All authors critically revised the manuscript for important intelligent content.

COMPETING INTERESTS

E.R. is a cofounder of Medaware Ltd. (https://www.medaware.com/) and Metabomed (https://www.metabomed.com/), a cofounder and nonpaid scientific consultant of Pangea Biomed (https://pangeamedicine.com/), and a scientific advisory board member of

899 GlaxoSmithKline Oncology (https://us.gsk.com/en-us/company/oncology/). The remaining
900 authors declare no conflicts of interest.
901

REFERENCES

[1] Tsimberidou, A. M., Fountzilas, E., Nikanjam, M., & Kurzrock, R. (2020). Review of precision cancer medicine: Evolution of the treatment paradigm. Cancer treatment reviews, 86, 102019.

[2] Huang K, Xiao C, Glass LM, Critchlow CM,. Machine learning applications for therapeutic tasks with genomics data. Patterns 2021; 2(10):100328.

[3] Fisher, B., Brown, A., Mamounas, E., Wieand, S., Robidoux, A., Margolese, R. G., … & Dimitrov, N. V. (1997). Effect of preoperative chemotherapy on local-regional disease in women with operable breast cancer: findings from National Surgical Adjuvant Breast and Bowel Project B-18. Journal of clinical oncology, 15(7), 2483-2493.

[4] Bear, H. D., Anderson, S., Brown, A., Smith, R., Mamounas, E. P., Fisher, B., ... & Wolmark, N. (2003). The effect on tumor response of adding sequential preoperative docetaxel to preoperative doxorubicin and cyclophosphamide: preliminary results from National Surgical Adjuvant Breast and Bowel Project Protocol B-27. Journal of Clinical Oncology, 21(22), 4165-4174.

[5] Golshan, M., Loibl, S., Wong, S. M., Huober, J. B., O'Shaughnessy, J., Rugo, H. S., ... & Untch, M. (2020). Breast conservation after neoadjuvant chemotherapy for triple-negative breast cancer: surgical results from the BrighTNess randomized clinical trial. JAMA surgery, 155(3), e195410-e195410.

[6] Urueña, C., Lasso, P., Bernal-Estevez, D. et al. The breast cancer immune microenvironment is modified by neoadjuvant chemotherapy. Sci Rep 12, 7981 (2022). https://doi.org/10.1038/s41598-022-12108-5

[7] Ali, H. R., Dariush, A., Provenzano, E., Bardwell, H., Abraham, J. E., Iddawela, M., ... & Caldas, C. (2016). Computational pathology of pre-treatment biopsies identifies lymphocyte density as a predictor of response to neoadjuvant chemotherapy in breast cancer. Breast Cancer Research, 18(1), 1-11.

[8] Ali, H. R., Dariush, A., Thomas, J., Provenzano, E., Dunn, J., Hiller, L., ... & Caldas, C. (2017). Lymphocyte density determined by computational pathology validated as a predictor of

930 response to neoadjuvant chemotherapy in breast cancer: secondary analysis of the
931 ARTemis trial. Annals of Oncology, 28(8), 1832-1835.
932 [9] Dieci, M. V., Prat, A., Tagliafico, E., Paré, L., Ficarra, G., Bisagni, G., ... & Guarneri, V. (2016).
933 Integrated evaluation of PAM50 subtypes and immune modulation of pCR in HER2-positive
934 breast cancer patients treated with chemotherapy and HER2-targeted agents in the
935 CherLOB trial. Annals of Oncology, 27(10), 1867-1873.
936 [10] Griguolo, G., Serna, G., Pascual, T. et al. Immune microenvironment characterisation and
937 dynamics during anti-HER2-based neoadjuvant treatment in HER2-positive breast cancer.
938 npj Precis. Onc. 5, 23 (2021). HYPERLINK "https://doi.org/10.1038/s41698-021-00163-6.
939 https://doi.org/10.1038/s41698-021-00163-64040
940 [11] Sammut, SJ., Crispin-Ortuzar, M., Chin, Sf. et al. Multi-omic machine learning predictor of
941 breast cancer therapy response. Nature 601, 623–629 (2022).
942 https://doi.org/10.1038/s41586-021-04278-5
943 [12] Klemm F, Joyce JA. Microenvironmental regulation of therapeutic response in cancer.
944 Trends Cell Biol. 2015 Apr;25(4):198-213. doi: 10.1016/j.tcb.2014.11.006. Epub 2014 Dec
945 22. PMID: 25540894; PMCID: PMC5424264.
946 [13] Son B, Lee S, Youn H, Kim E, Kim W, Youn B. The role of tumor microenvironment in
947 therapeutic resistance. Oncotarget. 2017 Jan 17;8(3):3933-3945. doi:
948 10.18632/oncotarget.13907. PMID: 27965469; PMCID: PMC5354804.
949 [14] Wu, P., Gao, W., Su, M., Nice, E. C., Zhang, W., Lin, J., & Xie, N. (2021). Adaptive
950 mechanisms of tumor therapy resistance driven by tumor microenvironment. Frontiers in
951 cell and developmental biology, 9, 641469.
952 [15] Mehraj, U., Dar, A.H., Wani, N.A. et al. Tumor microenvironment promotes breast cancer
953 chemoresistance. Cancer Chemother Pharmacol 87, 147–158 (2021).
954 https://doi.org/10.1007/s00280-020-04222-w
955 [16] Ruffell, B., & Coussens, L. M. (2015). Macrophages and therapeutic resistance in cancer.
956 Cancer cell, 27(4), 462-472.

957 [17] Acharyya, S., Oskarsson, T., Vanharanta, S., Malladi, S., Kim, J., Morris, P. G., ... & Massagué,
958 J. (2012). A CXCL1 paracrine network links cancer chemoresistance and metastasis. Cell,
959 150(1), 165-178.
960 [18] Li, M., Quintana, A., Alberts, E., Hung, M. S., Boulat, V., Ripoll, M. M., & Grigoriadis, A.
961 (2023). B Cells in Breast Cancer Pathology. Cancers, 15(5), 1517.
962 [19] Sakaguchi, A., Horimoto, Y., Onagi, H. et al. Plasma cell infiltration and treatment effect in
963 breast cancer patients treated with neoadjuvant chemotherapy. Breast Cancer Res 23, 99
964 (2021). https://doi.org/10.1186/s13058-021-01477-w
965 [20] Yeong, J., Lim, J. C. T., Lee, B., Li, H., Chia, N., Ong, C. C. H., ... & Iqbal, J. (2018). High
966 densities of tumor-associated plasma cells predict improved prognosis in triple negative
967 breast cancer. Frontiers in immunology, 9, 1209.
968 [21] Bhinder, B., Gilvary, C., Madhukar, N. S., & Elemento, O. (2021). Artificial intelligence in
969 cancer research and precision medicine. Cancer Discovery, 11(4), 900-915.
970 [22] Singla, N., & Singla, S. (2020). Harnessing big data with machine learning in precision
971 oncology. Kidney cancer journal: official journal of the Kidney Cancer Association, 18(3), 83.
972 [23] Senft, D., Leiserson, M. D., Ruppin, E., & Ze'ev, A. R. (2017). Precision oncology: the road
973 ahead. *Trends in molecular medicine*, *23*(10), 874-898.
974 [24] Tsimberidou, A. M., Fountzilas, E., Bleris, L., & Kurzrock, R. (2020, September).
975 Transcriptomics and solid tumors: The next frontier in precision cancer medicine. In
976 Seminars in cancer biology. Academic Press.
977 [25] Siravegna, G., Marsoni, S., Siena, S., & Bardelli, A. (2017). Integrating liquid biopsies into the
978 management of cancer. Nature reviews Clinical oncology, 14(9), 531-548.
979 [26] Heitzer, E., Haque, I. S., Roberts, C. E., & Speicher, M. R. (2019). Current and future
980 perspectives of liquid biopsies in genomics-driven oncology. Nature Reviews Genetics,
981 20(2), 71-88.
982 [27] Sawabata, N. (2020). Circulating tumor cells: From the laboratory to the cancer clinic.
983 Cancers, 12(10), 3065.

984 [28] Beaubier, N., Bontrager, M., Huether, R., Igartua, C., Lau, D., Tell, R., ... & White, K. P.
985 (2019). Integrated genomic profiling expands clinical options for patients with
986 cancer. *Nature biotechnology*, *37*(11), 1351-1360.
987 [29] Hayashi, H., Takiguchi, Y., Minami, H., Akiyoshi, K., Segawa, Y., Ueda, H., ... & Nakagawa, K.
988 (2020). Site-specific and targeted therapy based on molecular profiling by next-generation
989 sequencing for cancer of unknown primary site: a nonrandomized phase 2 clinical trial.
990 JAMA oncology, 6(12), 1931-1938.
991 [30] Vaske, O. M., Bjork, I., Salama, S. R., Beale, H., Shah, A. T., Sanders, L., ... & Haussler, D.
992 (2019). Comparative tumor RNA sequencing analysis for difficult-to-treat pediatric and
993 young adult patients with cancer. *JAMA network open*, *2*(10), e1913968-e1913968.
994 [31] Lee, J. S., Nair, N. U., Dinstag, G., Chapman, L., Chung, Y., Wang, K., ... & Ruppin, E. (2021).
995 Synthetic lethality-mediated precision oncology via the tumor transcriptome. Cell, 184(9),
996 2487-2502.
997 [32] Sinha, S., Dhruba, S. R., Wu, W., Kerr, D. L., Stroganov, O. V., Grishagin, I., ... & Ruppin, E.
998 (2022). Predicting patient treatment response and resistance via single-cell transcriptomics
999 of their tumors. bioRxiv.
1000 [33] Dinstag, G., Shulman, E. D., Elis, E., Ben-Zvi, D. S., Tirosh, O., Maimon, E., ... & Aharonov, R.
1001 (2022). Clinically oriented prediction of patient response to targeted and immunotherapies
1002 from the tumor transcriptome. bioRxiv.
1003 [34] Fu, Y., Jung, A. W., Torne, R. V., Gonzalez, S., Vöhringer, H., Shmatko, A., ... & Gerstung, M.
1004 (2020). Pan-cancer computational histopathology reveals mutations, tumor composition
1005 and prognosis. Nature Cancer, 1(8), 800-810.
1006 [35] Noorbakhsh, J., Farahmand, S., Namburi, S., Caruana, D., Rimm, D., Soltanieh-ha, M., ... &
1007 Chuang, J. H. (2020). Deep learning-based cross-classifications reveal conserved spatial
1008 behaviors within tumor histological images. Nature communications, 11(1), 1-14.
1009 [36] Yu, K. H., Wang, F., Berry, G. J., Re, C., Altman, R. B., Snyder, M., & Kohane, I. S. (2020).
1010 Classifying non-small cell lung cancer types and transcriptomic subtypes using
1011 convolutional neural networks. Journal of the American Medical Informatics Association,
1012 27(5), 757-769.

1013 [37] Couture, H. D., Williams, L. A., Geradts, J., Nyante, S. J., Butler, E. N., Marron, J. S., ... &
1014 Niethammer, M. (2018). Image analysis with deep learning to predict breast cancer grade,
1015 ER status, histologic subtype, and intrinsic subtype. NPJ breast cancer, 4(1), 1-8.
1016 [38] Qu, H., Zhou, M., Yan, Z., Wang, H., Rustgi, V. K., Zhang, S., ... & Metaxas, D. N. (2021).
1017 Genetic mutation and biological pathway prediction based on whole slide images in breast
1018 carcinoma using deep learning. NPJ precision oncology, 5(1), 1-11.
1019 [39] Hoang, D. T., Dinstag, G., Hermida, L. C., Ben-Zvi, D. S., Elis, E., Caley, K., ... & Ruppin, E.
1020 (2022). Synthetic lethality-based prediction of cancer treatment response from
1021 histopathology images. bioRxiv.
1022 [40] Tanioka, M., Fan, C., Parker, J. S., Hoadley, K. A., Hu, Z., Li, Y., ... & Perou, C. M. (2018).
1023 Integrated Analysis of RNA and DNA from the Phase III Trial CALGB 40601 Identifies
1024 Predictors of Response to Trastuzumab-Based Neoadjuvant Chemotherapy in HER2-
1025 Positive Breast CancerIntegrated Response Models in HER2-Positive Breast Cancer. Clinical
1026 Cancer Research, 24(21), 5292-5304.
1027 [41] Wong, M., Mayoh, C., Lau, L., Khuong-Quang, D. A., Pinese, M., Kumar, A., ... & Cowley, M.
1028 J. (2020). Whole genome, transcriptome and methylome profiling enhances actionable
1029 target discovery in high-risk pediatric cancer. Nature medicine, 26(11), 1742-1753.
1030 [42] Rodon, J., Soria, J. C., Berger, R., Miller, W. H., Rubin, E., Kugel, A., ... & Kurzrock, R. (2019).
1031 Genomic and transcriptomic profiling expands precision cancer medicine: the WINTHER
1032 trial. Nature medicine, 25(5), 751-758.
1033 [43] Korde, L. A., Somerfield, M. R., Carey, L. A., Crews, J. R., Denduluri, N., Hwang, E. S., ... &
1034 Hershman, D. L. (2021). Neoadjuvant chemotherapy, endocrine therapy, and targeted
1035 therapy for breast cancer: ASCO guideline. Journal of Clinical Oncology, 39(13), 1485-1505.
1036 [44] Kester, L., Seinstra, D., van Rossum, A. G., Vennin, C., Hoogstraat, M., van der Velden, D., ...
1037 & van Rheenen, J. (2022). Differential Survival and Therapy Benefit of Patients with Breast
1038 Cancer Are Characterized by Distinct Epithelial and Immune Cell Microenvironments Tumor
1039 Cellular Composition Predicts Benefit to Therapies. *Clinical Cancer Research*, OF1-OF12.
1040 [45] Wang, K., Patkar, S., Lee, J.S., Gertz, E.M., Robinson, W., Schischlik, F., Crawford, D.R.,
1041 Schäffer, A.A. and Ruppin, E. (2022). Deconvolving Clinically Relevant Cellular Immune

1042 Cross-talk from Bulk Gene Expression Using CODEFACS and LIRICS Stratifies Patients with
1043 Melanoma to Anti–PD-1 Therapy. Cancer discovery, 12(4), 1088-1105.
1044 [46] Wu, S. Z., Al-Eryani, G., Roden, D. L., Junankar, S., Harvey, K., Andersson, A., ... & Swarbrick,
1045 A. (2021). A single-cell and spatially resolved atlas of human breast cancers. *Nature*
1046 *genetics*, *53*(9), 1334-1347.
1047 [47] Earl, H. M., Hiller, L., Dunn, J. A., Blenkinsop, C., Grybowicz, L., Vallier, A. L., ... & Hayward,
1048 L. (2015). Efficacy of neoadjuvant bevacizumab added to docetaxel followed by
1049 fluorouracil, epirubicin, and cyclophosphamide, for women with HER2-negative early
1050 breast cancer (ARTemis): an open-label, randomised, phase 3 trial. The lancet oncology,
1051 16(6), 656-666.
1052 [48] Loibl, S., O'Shaughnessy, J., Untch, M., Sikov, W. M., Rugo, H. S., McKee, M. D., ... & Geyer
1053 Jr, C. E. (2018). Addition of the PARP inhibitor veliparib plus carboplatin or carboplatin
1054 alone to standard neoadjuvant chemotherapy in triple-negative breast cancer (BrighTNess):
1055 a randomised, phase 3 trial. The Lancet Oncology, 19(4), 497-509.
1056 [49] Zhang, Y., Chen, H., Mo, H., Hu, X., Gao, R., Zhao, Y., ... & Liu, Z. (2021). Single-cell analyses
1057 reveal key immune cell subsets associated with response to PD-L1 blockade in triple-
1058 negative breast cancer. Cancer Cell, 39(12), 1578-1593.
1059 [50] Bassez, A., Vos, H., Van Dyck, L., Floris, G., Arijs, I., Desmedt, C., ... & Lambrechts, D. (2021).
1060 A single-cell map of intratumoral changes during anti-PD1 treatment of patients with
1061 breast cancer. *Nature medicine*, *27*(5), 820-832.
1062 [51] Ramilowski, J., Goldberg, T., Harshbarger, J. *et al.* A draft network of ligand–receptor-
1063 mediated multicellular signalling in human. *Nat Commun* **6**, 7866 (2015).
1064 https://doi.org/10.1038/ncomms8866
1065 [52] Green, D. R., Ferguson, T., Zitvogel, L., & Kroemer, G. (2009). Immunogenic and tolerogenic
1066 cell death. Nature Reviews Immunology, 9(5), 353-363.
1067 [53] Fabregat, A. et al. The Reactome Pathway Knowledgebase. Nucleic Acids Res. 46, D649–
1068 D655 (2018).
1069 [54] Molinari, M. (2000). Cell cycle checkpoints and their inactivation in human cancer. Cell
1070 proliferation, 33(5), 261-274.

1071 [55] Bower, J.J., Vance, L.D., Psioda, M. et al. Patterns of cell cycle checkpoint deregulation
1072 associated with intrinsic molecular subtypes of human breast cancer cells. npj Breast
1073 Cancer 3, 9 (2017). https://doi.org/10.1038/s41523-017-0009-7
1074 [56] Zhou, K., Sun, Y., Dong, D. et al. EMP3 negatively modulates breast cancer cell DNA
1075 replication, DNA damage repair, and stem-like properties. Cell Death Dis 12, 844 (2021).
1076 https://doi.org/10.1038/s41419-021-04140-6
1077 [57] Repo, H., Löyttyniemi, E., Kurki, S. et al. A prognostic model based on cell-cycle control
1078 predicts outcome of breast cancer patients. BMC Cancer 20, 558 (2020).
1079 https://doi.org/10.1186/s12885-020-07045-3
1080 [58] Vihervuori, H., Korpinen, K., Autere, T. A., Repo, H., Talvinen, K., & Kronqvist, P. (2022).
1081 Varying outcomes of triple-negative breast cancer in different age groups–prognostic value
1082 of clinical features and proliferation. Breast Cancer Research and Treatment, 1-12.
1083 [59] Thu, K. L., Soria-Bretones, I., Mak, T. W., & Cescon, D. W. (2018). Targeting the cell cycle in
1084 breast cancer: towards the next phase. Cell Cycle, 17(15), 1871-1885.
1085 [60] Zhang, J., Chan, D. W., & Lin, S. Y. (2022). Exploiting DNA Replication Stress as a Therapeutic
1086 Strategy for Breast Cancer. Biomedicines, 10(11), 2775.
1087 [61] Zhu, X., & Zhou, W. (2015). The emerging regulation of VEGFR-2 in triple-negative breast
1088 cancer. Frontiers in Endocrinology, 6, 159.
1089 [62] Ceci, C., Atzori, M. G., Lacal, P. M., & Graziani, G. (2020). Role of VEGFs/VEGFR-1 signaling
1090 and its inhibition in modulating tumor invasion: Experimental evidence in different
1091 metastatic cancer models. International journal of molecular sciences, 21(4), 1388.
1092 [63] Zhang, Q., Lu, S., Li, T., Yu, L., Zhang, Y., Zeng, H., ... & Lin, Y. (2019). ACE2 inhibits breast
1093 cancer angiogenesis via suppressing the VEGFa/VEGFR2/ERK pathway. Journal of
1094 Experimental & Clinical Cancer Research, 38(1), 1-12.
1095 [64] Edwards, A., & Brennan, K. (2021). Notch signalling in breast development and cancer.
1096 Frontiers in Cell and Developmental Biology, 9, 692173.
1097 [65] Zhou, B., Lin, W., Long, Y. *et al.* Notch signaling pathway: architecture, disease, and
1098 therapeutics. *Sig Transduct Target Ther* **7**, 95 (2022). https://doi.org/10.1038/s41392-022-
1099 00934-y.

1100 [66] Miao, K., Lei, J.H., Valecha, M.V. et al. NOTCH1 activation compensates BRCA1 deficiency
1101 and promotes triple-negative breast cancer formation. Nat Commun 11, 3256 (2020).
1102 https://doi.org/10.1038/s41467-020-16936-9
1103 [67] BeLow, M., & Osipo, C. (2020). Notch signaling in breast cancer: a role in drug resistance.
1104 Cells, 9(10), 2204.
1105 [68] Li, L., Wang, X., Hu, K. et al. ZNF133 is a potent suppressor in breast carcinogenesis through
1106 dampening L1CAM, a driver for tumor progression. Oncogene (2023).
1107 https://doi.org/10.1038/s41388-023-02731-5
1108 [69] van der Maten, M., Reijnen, C., Pijnenborg, J. M., & Zegers, M. M. (2019). L1 cell adhesion
1109 molecule in cancer, a systematic review on domain-specific functions. International journal
1110 of molecular sciences, 20(17), 4180.
1111 [70] Zhang, J., Yang, F., Ding, Y., Zhen, L., Han, X., Jiao, F., & Tang, J. (2015). Overexpression of L1
1112 cell adhesion molecule correlates with aggressive tumor progression of patients with
1113 breast cancer and promotes motility of breast cancer cells. International journal of clinical
1114 and experimental pathology, 8(8), 9240.
1115 [71] Bandola-Simon, J., & Roche, P. A. (2019). Dysfunction of antigen processing and
1116 presentation by dendritic cells in cancer. Molecular immunology, 113, 31-37.
1117 [72] Dhatchinamoorthy, K., Colbert, J. D., & Rock, K. L. (2021). Cancer immune evasion through
1118 loss of MHC class I antigen presentation. Frontiers in immunology, 12, 636568.
1119 [73] McDonnell, A. M., Lesterhuis, W. J., Khong, A., Nowak, A. K., Lake, R. A., Currie, A. J., &
1120 Robinson, B. W. (2015). Tumor-infiltrating dendritic cells exhibit defective
1121 cross-presentation of tumor antigens, but is reversed by chemotherapy. European journal
1122 of immunology, 45(1), 49-59.
1123 [74] Galluzzi, L., Humeau, J., Buqué, A., Zitvogel, L., & Kroemer, G. (2020). Immunostimulation
1124 with chemotherapy in the era of immune checkpoint inhibitors. Nature reviews Clinical
1125 oncology, 17(12), 725-741.
1126 [75] Sahni, S., Wang, B., Wu, D., Dhruba, S. R., Nagy, M., Patkar, S., ... & Ruppin, E. (2024). A
1127 machine learning model reveals expansive downregulation of ligand-receptor interactions

1128 that enhance lymphocyte infiltration in melanoma with developed resistance to immune
1129 checkpoint blockade. Nature Communications, 15(1), 8867.
1130 [76] Szklarczyk, D., Gable, A. L., Lyon, D., Junge, A., Wyder, S., Huerta-Cepas, J., ... & Mering, C.
1131 V. (2019). STRING v11: protein–protein association networks with increased coverage,
1132 supporting functional discovery in genome-wide experimental datasets. Nucleic acids
1133 research, 47(D1), D607-D613.
1134 [77] Li, J., Li, C., Liu, X. et al. GDF9 concentration in embryo culture medium is linked to human
1135 embryo quality and viability. J Assist Reprod Genet 39, 117–125 (2022).
1136 https://doi.org/10.1007/s10815-021-02368-x
1137 [78] Stocker, W. A., Walton, K. L., Richani, D., Chan, K. L., Beilby, K. H., Finger, B. J., ... &
1138 Harrison, C. A. (2020). A variant of human growth differentiation factor-9 that improves
1139 oocyte developmental competence. Journal of Biological Chemistry, 295(23), 7981-7991.
1140 [79] Gomez-Puerto, M. C., Iyengar, P. V., García de Vinuesa, A., Ten Dijke, P., &
1141 Sanchez-Duffhues, G. (2019). Bone morphogenetic protein receptor signal transduction in
1142 human disease. The journal of pathology, 247(1), 9-20.
1143 [80] Feary, E. S., Juengel, J. L., Smith, P., French, M. C., O'Connell, A. R., Lawrence, S. B., ... &
1144 McNatty, K. P. (2007). Patterns of expression of messenger RNAs encoding GDF9, BMP15,
1145 TGFBR1, BMPR1B, and BMPR2 during follicular development and characterization of
1146 ovarian follicular populations in ewes carrying the Woodlands FecX2W mutation. Biology of
1147 reproduction, 77(6), 990-998.
1148 [81] Hanavadi, S., Martin, T. A., Watkins, G., Mansel, R. E., & Jiang, W. G. (2007). The role of
1149 growth differentiation factor-9 (GDF-9) and its analog, GDF-9b/BMP-15, in human breast
1150 cancer. Annals of surgical oncology, 14, 2159-2166.
1151 [82] Harrath, A. H., Jalouli, M., Oueslati, M. H., Farah, M. A., Feriani, A., Aldahmash, W., ... &
1152 Alwasel, S. (2021). The flavonoid, kaempferol-3-O-apiofuranosyl-7-O-rhamnopyranosyl, as
1153 a potential therapeutic agent for breast cancer with a promoting effect on ovarian
1154 function. Phytotherapy Research, 35(11), 6170-6180.
1155 [83] Bach, D. H., Park, H. J., & Lee, S. K. (2018). The dual role of bone morphogenetic proteins in
1156 cancer. Molecular Therapy-Oncolytics, 8, 1-13.

1157 [84] Bokobza, S. M., Ye, L., Kynaston, H. E., Mansel, R. E., & Jiang, W. G. (2009). Reduced
1158 expression of BMPR-IB correlates with poor prognosis and increased proliferation of breast
1159 cancer cells. Cancer genomics & proteomics, 6(2), 101-108.
1160 [85] Zheng, Y., Jiang, X., Wang, M., Yang, S., Deng, Y., Li, Y., ... & Chen, L. (2022). BMPR1B
1161 Polymorphisms (rs1434536 and rs1970801) are Associated With Breast Cancer
1162 Susceptibility in Northwest Chinese Han Females: A Case-Control Study. Clinical Breast
1163 Cancer, 22(5), e641-e646.
1164 [86] Dai, K., Qin, F., Zhang, H., Liu, X., Guo, C., Zhang, M., ... & Ma, Y. (2016). Low expression of
1165 BMPRIB indicates poor prognosis of breast cancer and is insensitive to taxane-anthracycline
1166 chemotherapy. Oncotarget, 7(4), 4770.
1167 [87] Jing, S., Wen, D., Yu, Y., Holst, P. L., Luo, Y., Fang, M., ... & Fox, G. M. (1996). GDNF–induced
1168 activation of the ret protein tyrosine kinase is mediated by GDNFR-α, a novel receptor for
1169 GDNF. Cell, 85(7), 1113-1124.
1170 [88] Fielder, G. C., Yang, T. W. S., Razdan, M., Li, Y., Lu, J., Perry, J. K., ... & Liu, D. X. (2018). The
1171 GDNF family: a role in cancer?. Neoplasia, 20(1), 99-117.
1172 [89] Li, Q., Cao, Z., & Zhao, S. (2022). The Emerging Portrait of Glial Cell Line-derived
1173 Neurotrophic Factor Family Receptor Alpha (GFRα) in Cancers. International Journal of
1174 Medical Sciences, 19(4), 659.
1175 [90] Pecar, G., Liu, S., Hooda, J. et al. RET signaling in breast cancer therapeutic resistance and
1176 metastasis. Breast Cancer Res 25, 26 (2023). https://doi.org/10.1186/s13058-023-01622-7
1177 [91] Horibata, S., Rice, E. J., Mukai, C., Marks, B. A., Sams, K., Zheng, H., ... & Danko, C. G. (2018).
1178 ER-positive breast cancer cells are poised for RET-mediated endocrine resistance. PLoS
1179 One, 13(4), e0194023.
1180 [92] Bhakta, S., Crocker, L. M., Chen, Y., Hazen, M., Schutten, M. M., Li, D., ... & Junutula, J. R.
1181 (2018). An Anti-GDNF Family Receptor Alpha 1 (GFRA1) Antibody–Drug Conjugate for the
1182 Treatment of Hormone Receptor–Positive Breast Cancer Targeting Hormone-Positive
1183 Breast Cancer with a GFRA1 ADC. Molecular cancer therapeutics, 17(3), 638-649.
1184 [93] Kim, M., & Kim, D. J. (2018). GFRA1: a novel molecular target for the prevention of
1185 osteosarcoma chemoresistance. International journal of molecular sciences, 19(4), 1078.

1186 [94] Liu, H., Yang, Z., Lu, W., Chen, Z., Chen, L., Han, S., ... & Cai, Y. (2020). Chemokines and
1187 chemokine receptors: A new strategy for breast cancer therapy. Cancer medicine, 9(11),
1188 3786-3799.
1189 [95] Liang, Y., Yi, L., Liu, P., Jiang, L., Wang, H., Hu, A., ... & Dong, J. (2018). CX3CL1 involves in
1190 breast cancer metastasizing to the spine via the Src/FAK signaling pathway. Journal of
1191 Cancer, 9(19), 3603.
1192 [96] Tardáguila, M., Mira, E., García-Cabezas, M. A., Feijoo, A. M., Quintela-Fandino, M.,
1193 Azcoitia, I., ... & Manes, S. (2013). CX3CL1 Promotes Breast Cancer via Transactivation of
1194 the EGF PathwayCX3CL1 Promotes Breast Cancer. Cancer research, 73(14), 4461-4473.
1195 [97] Jamieson-Gladney, W.L., Zhang, Y., Fong, A.M. et al. The chemokine receptor CX3CR1 is
1196 directly involved in the arrest of breast cancer cells to the skeleton. Breast Cancer Res 13,
1197 R91 (2011). https://doi.org/10.1186/bcr3016
1198 [98] Rivas-Fuentes, S., Salgado-Aguayo, A., Arratia-Quijada, J., & Gorocica-Rosete, P. (2021).
1199 Regulation and biological functions of the CX3CL1-CX3CR1 axis and its relevance in solid
1200 cancer: A mini-review. Journal of Cancer, 12(2), 571.
1201 [99] Yue, Y., Zhang, Q., & Sun, Z. (2022). CX3CR1 acts as a protective biomarker in the tumor
1202 microenvironment of colorectal Cancer. Frontiers in Immunology, 12, 5972.
1203 [100] Ishida, Y., Kuninaka, Y., Yamamoto, Y., Nosaka, M., Kimura, A., Furukawa, F., ... & Kondo,
1204 T. (2020). Pivotal involvement of the CX3CL1-CX3CR1 axis for the recruitment of M2 tumor-
1205 associated macrophages in skin carcinogenesis. *Journal of Investigative*
1206 *Dermatology*, *140*(10), 1951-1961.
1207 [101] Cortes, J., Haiderali, A., Huang, M., Pan, W., Schmid, P., Akers, K. G., ... & O'Shaughnessy,
1208 J. (2023). Neoadjuvant immunotherapy and chemotherapy regimens for the treatment of
1209 high-risk, early-stage triple-negative breast cancer: a systematic review and network meta-
1210 analysis. *BMC cancer*, *23*(1), 792.
1211 [102] Schmid, P., Cortes, J., Pusztai, L., McArthur, H., Kümmel, S., Bergh, J., ... &
1212 O'Shaughnessy, J. (2020). Pembrolizumab for early triple-negative breast cancer. *New*
1213 *England Journal of Medicine*, *382*(9), 810-821.

1214 [103] Kim, L., Coman, M., Pusztai, L., & Park, T. S. (2023). Neoadjuvant Immunotherapy in
1215 Early, Triple-Negative Breast Cancers: Catching Up with the Rest. *Annals of Surgical*
1216 *Oncology*, *30*(11), 6441-6449.
1217 [104] Michaud, M., Martins, I., Sukkurwala, A. Q., Adjemian, S., Ma, Y., Pellegatti, P., ... &
1218 Kroemer, G. (2011). Autophagy-dependent anticancer immune responses induced by
1219 chemotherapeutic agents in mice. Science, 334(6062), 1573-1577.
1220 [105] Newman, A. M., Steen, C. B., Liu, C. L., Gentles, A. J., Chaudhuri, A. A., Scherer, F., ... &
1221 Alizadeh, A. A. (2019). Determining cell type abundance and expression from bulk tissues
1222 with digital cytometry. Nature biotechnology, 37(7), 773-782.
1223 [106] Han, Y., Wang, Y., Dong, X., Sun, D., Liu, Z., Yue, J., ... & Wang, C. (2023). TISCH2:
1224 expanded datasets and new tools for single-cell transcriptome analyses of the tumor
1225 microenvironment. Nucleic acids research, 51(D1), D1425-D1431.
1226 [107] Leon-Ferre, R. A., Jonas, S. F., Salgado, R., Loi, S., De Jong, V., Carter, J. M., ... &
1227 International Immuno-Oncology Biomarker Working Group. (2024). Tumor-Infiltrating
1228 Lymphocytes in Triple-Negative Breast Cancer. JAMA, 331(13), 1135-1144.
1229 [108] Ali, H. R., Chlon, L., Pharoah, P. D., Markowetz, F., & Caldas, C. (2016). Patterns of
1230 immune infiltration in breast cancer and their clinical implications: a gene-expression-
1231 based retrospective study. PLoS medicine, 13(12), e1002194.
1232 [109] Chowdhury, A., Pharoah, P. D., & Rueda, O. M. (2023). Evaluation and comparison of
1233 different breast cancer prognosis scores based on gene expression data. Breast Cancer
1234 Research, 25(1), 17.
1235 [110] Yu, Q., Li, Y. Y., & Chen, Y. (2025). scMalignantFinder distinguishes malignant cells in
1236 single-cell and spatial transcriptomics by leveraging cancer signatures. Communications
1237 Biology, 8(1), 504.
1238 [111] Patel, A. P., Tirosh, I., Trombetta, J. J., Shalek, A. K., Gillespie, S. M., Wakimoto, H., ... &
1239 Bernstein, B. E. (2014). Single-cell RNA-seq highlights intratumoral heterogeneity in primary
1240 glioblastoma. Science, 344(6190), 1396-1401.

1241 [112] Gao, R., Bai, S., Henderson, Y. C., Lin, Y., Schalck, A., Yan, Y., ... & Navin, N. E. (2021).
1242 Delineating copy number and clonal substructure in human tumors from single-cell
1243 transcriptomes. Nature biotechnology, 39(5), 599-608.
1244

SUPPLEMENTARY FIGURES

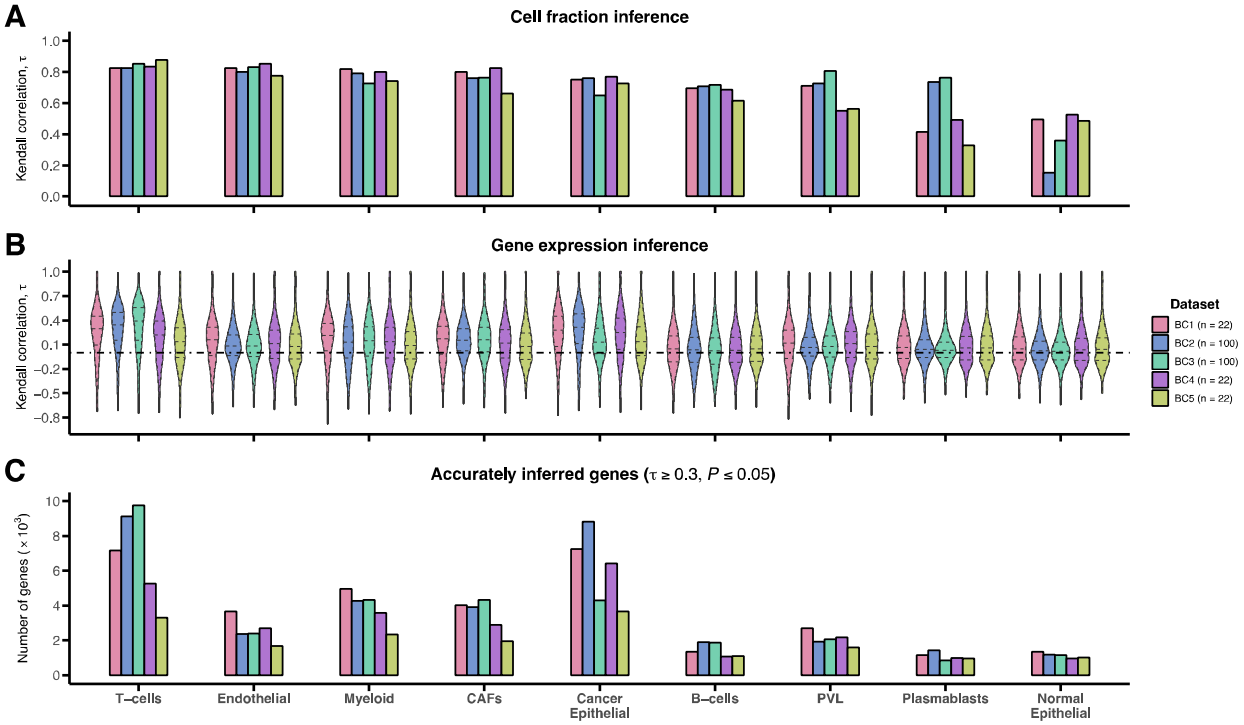

Supplementary Figure 1: Benchmarking CODEFACS on five breast cancer cohorts generated from single-cell (SC) data.

A. Correlation of actual and CODEFACS-inferred cell fraction values for nine cell types across five benchmark cohorts (BC1-5), generated *via* mixing SC expression from Wu et al. (see **METHODS**). Cell types are ranked by their mean correlation across the five cohorts in a descending order.

B. Correlation of actual and CODEFACS-inferred cell-type-specific gene expression values for nine cell types across five benchmark cohorts. Cell types are ranked by their mean correlation for cell abundance accuracy in **A**.

C. Number of accurately inferred genes for nine cell types across five benchmark cohorts. Cell types are ranked by their mean correlation for cell abundance accuracy in **A**.

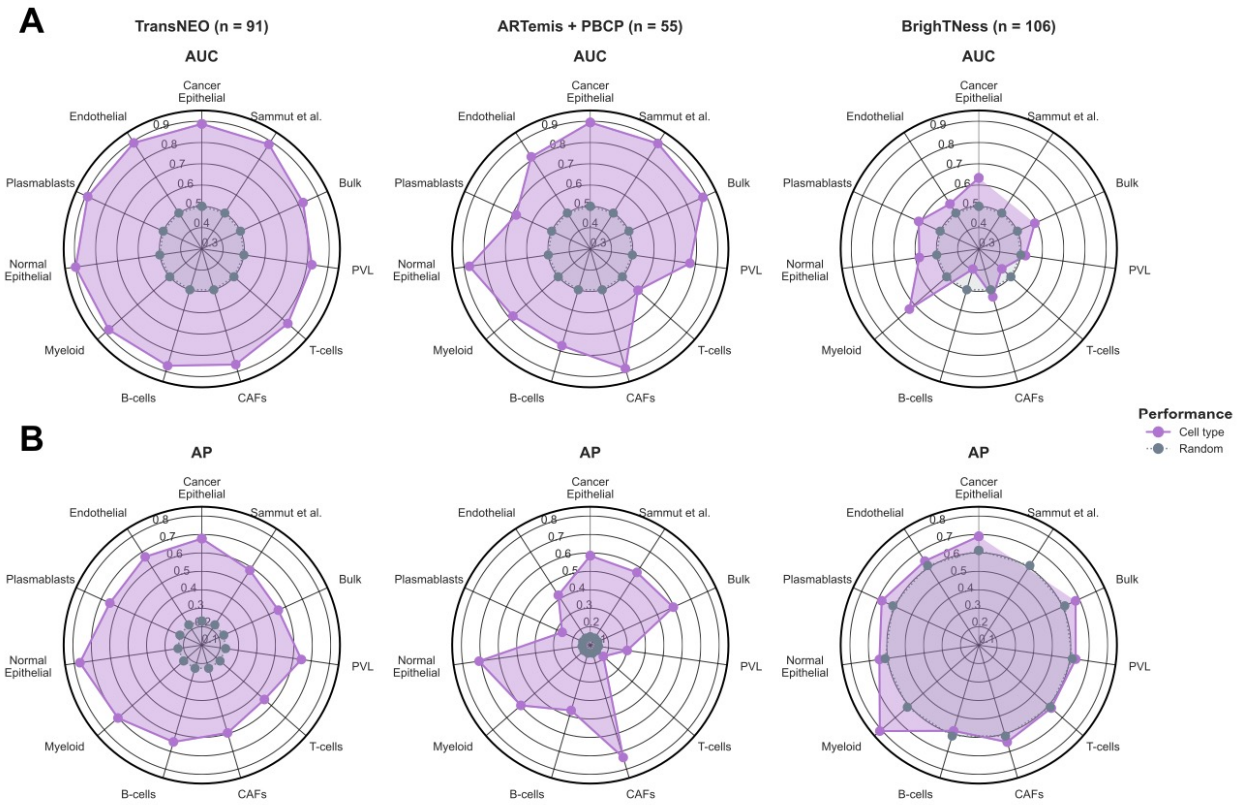

Supplementary Figure 2: Hyperparameter tuning with leave-one-out cross-validation (CV) leads to similar cell-type-specific performance to using three-fold cross-validation.

A-B. Comparison of model performance for nine cell-type-specific, bulk and Sammut et al. (for first two cohorts) predictors across TransNEO, ARTemis + PBCP and BrighTNess, where model hyperparameters were optimized using leave-one-out CV. AUC and AP stand for the area under the receiver operating characteristics curve and average precision, respectively. 'Random' denotes a random predictor (AUC = 0.5, AP = fraction of responders). Cell types are ranked by their original AUC values for TransNEO (obtained using three-fold CV for hyperparameter tuning; see **Figure 2A**) in the counterclockwise direction.

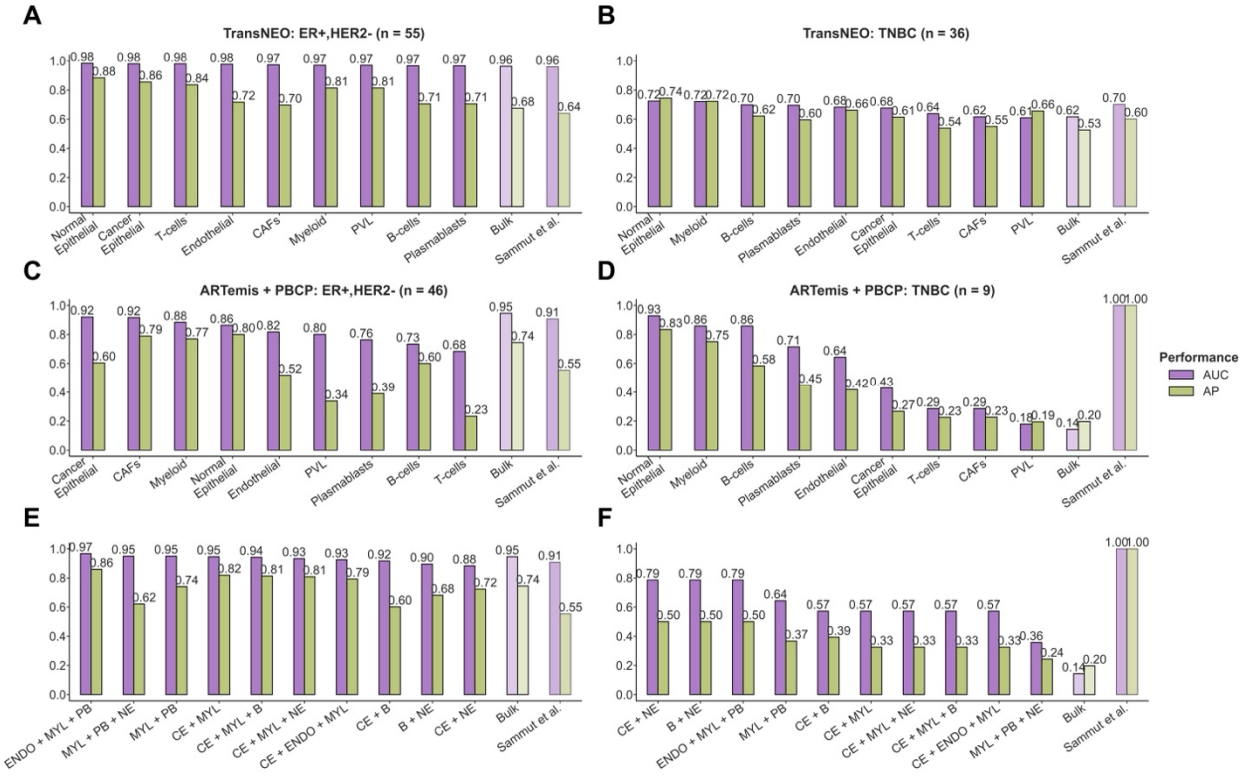

Supplementary Figure 3: The prominent cell types and ensembles mediating chemotherapy response in breast cancer tumor microenvironment in a subtype-specific manner.

A-B. Comparison of model performance across TransNEO for the ER+,HER2- (**A**) and TNBC (**B**) subtypes for nine cell-type-specific, bulk and Sammut et al. predictors. AUC and AP stand for the area under the receiver operating characteristics curve and average precision (equivalent to the area under the precision-recall curve), respectively. Cell types are ranked by their AUC values in a descending order.

C-D. Comparison of model performance across ARTemis + PBCP for the ER+,HER2- (**C**) and TNBC (**D**) subtypes for nine cell-type-specific, bulk and Sammut et al. predictors. Cell types are ranked by their AUC values in a descending order.

E-F. Comparison of model performance across with ARTemis + PBCP for the ER+,HER2- (**E**) and TNBC (**F**) subtypes for the five most prominent two-cell-ensembles, five most prominent three-cell-ensembles, bulk and Sammut et al. predictors. Ensembles are ranked by their AUC values in a descending order.

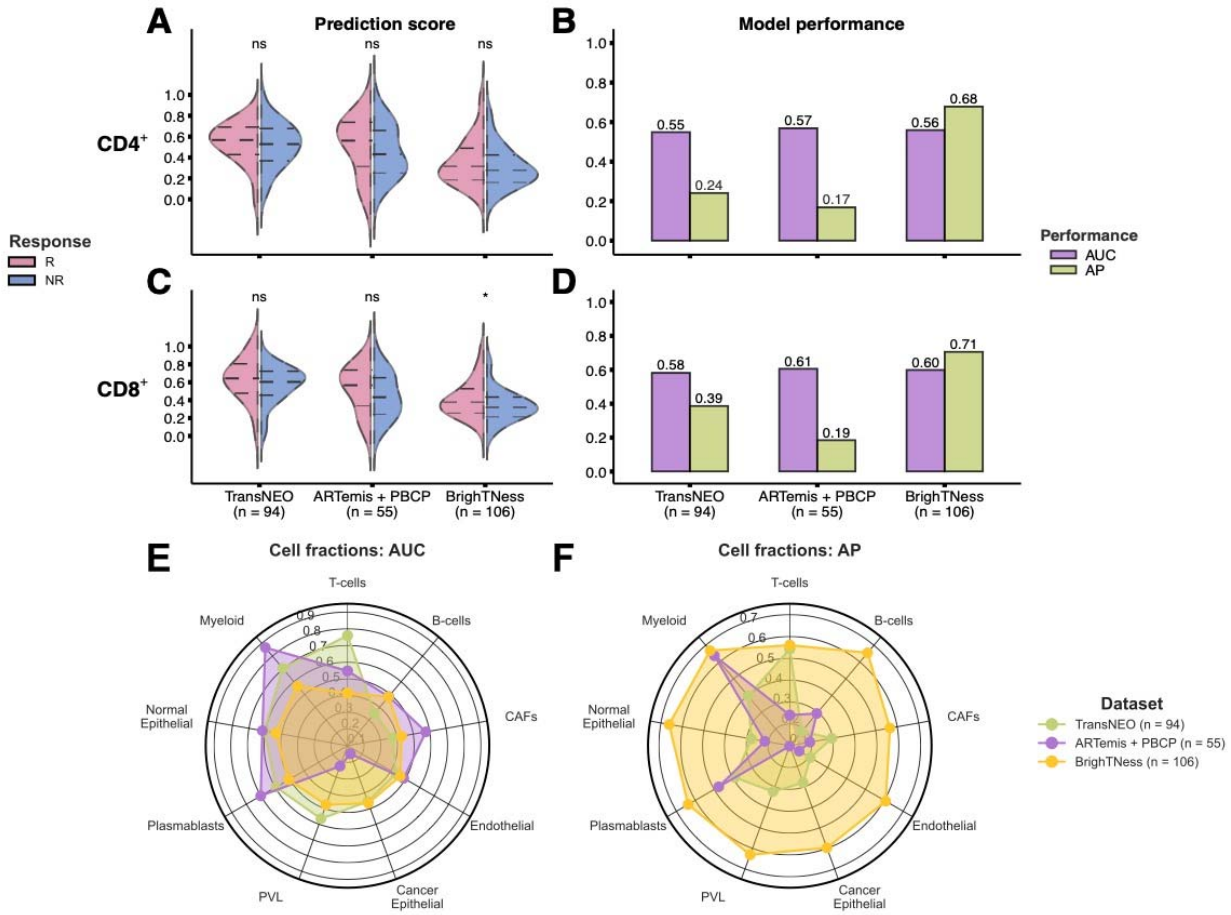

Supplementary Figure 4: The CD4$^+$ / CD8$^+$ T-cells enrichment and cell abundance – clinical response association analyses reaffirm the poor chemotherapy response stratification by T-cells at the current resolution.

A-B. GSVA enrichment scores (**A**) and predictive performance (**B**) of CD4$^+$ T-cells for chemotherapy response stratification across TransNEO, ARTemis + PBCP and BrighTNess. R and NR stand for responders and non-responders, respectively. The differences between the prediction scores were computed by using a one-tailed Wilcoxon rank-sum test (* and 'ns' denote $P \leq 0.05$ and $P > 0.05$, respectively). AUC and AP stand for the area under the receiver operating characteristics curve and average precision (equivalent to the area under precision-recall curve), respectively.

C-D. GSVA enrichment scores (**C**) and predictive performance (**D**) of CD8$^+$ T-cells for chemotherapy response stratification across the three cohorts.

1298 **E-F.** Predictive performance of abundances of the nine cell types across the three cohorts. Cell
1299 types are ranked by their AUC values for TransNEO in a descending order in the
1300 counterclockwise direction.
1301

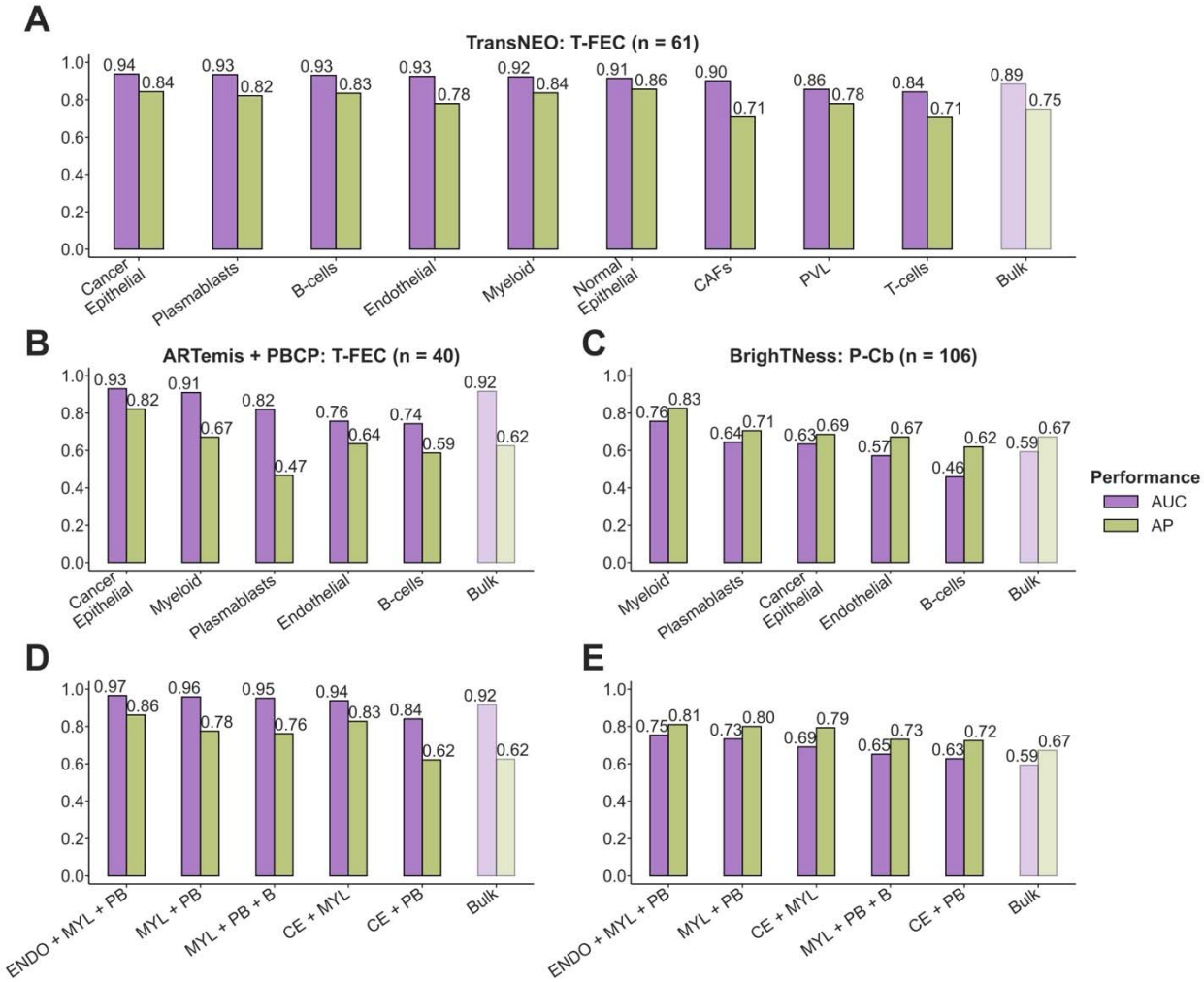

1302
1303 **Supplementary Figure 5: The prominent immune cell types and ensembles mediating**
1304 **response to the most prevalent immunogenic chemotherapy regimen in each breast cancer**
1305 **cohort.**
1306 **A.** Comparison of model performance for nine cell-type-specific and bulk predictors across
1307 TransNEO for the T-FEC regimen. AUC and AP stand for the area under the receiver operating
1308 characteristics curve and average precision (equivalent to the area under the precision-recall
1309 curve), respectively. *C*, *E*, *F* and *T* stand for cyclophosphamide, epirubicin, 5-flurouracil and

docetaxel (taxotere), respectively. Cell types are ranked by their AUC values in a descending order.

B-C. Comparison of model performance for the top five cell-type-specific and bulk predictors across ARTemis + PBCP for the T-FEC regiment (**B**) and BrighTNess for the paclitaxel – carboplatin (P-Cb) regimen (**C**). Cell types are ranked by their AUC values in a descending order.

D-E. Comparison of model performance for the top five multi-cell-type ensemble and bulk predictors across ARTemis + PBCP for the T-FEC regiment (**D**) and BrighTNess for the P-Cb regimen (**E**). Ensembles are ranked by their AUC values in a descending order.

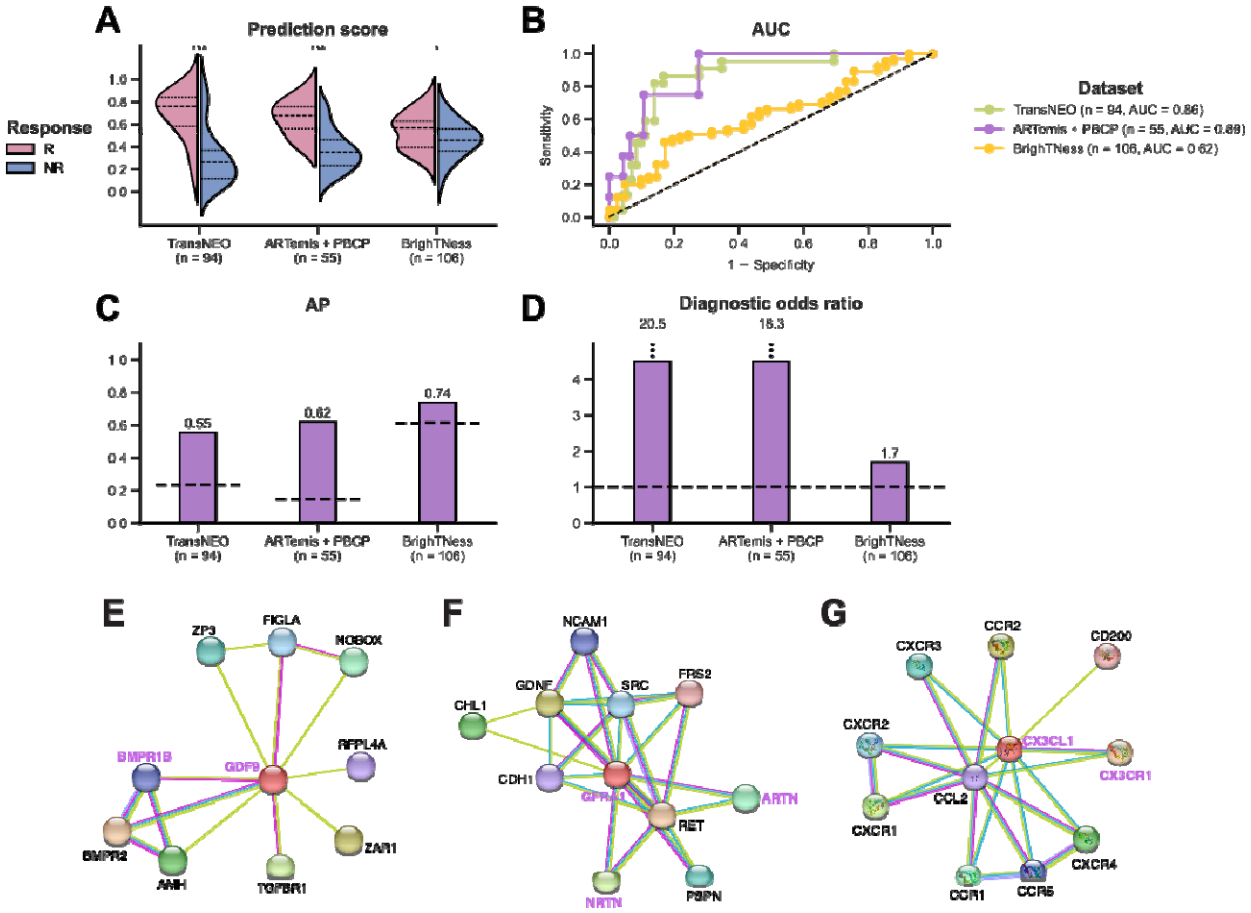

Supplementary Figure 6: Cell-cell interactions (CCIs) encompassing all cell types in mediating chemotherapy response in breast cancer tumor microenvironment.

A-D. Comparison of prediction scores (**A**) and model performance (**B-D**) for DECODEMi CCI-based predictor using all available CCIs across TransNEO, ARTemis + PBCP and BrighTNess. R and

NR stand for responders and non-responders, respectively. The differences between the prediction scores were computed by using a one-tailed Wilcoxon rank-sum test (*** and * denote $P \leq 0.001$ and $P \leq 0.05$, respectively). AUC and AP stand for the area under the receiver operating characteristics curve and average precision, respectively. The dotted lines in **C-D** represent the AP and diagnostic odds ratio (DOR) values for a random predictor (AP = fraction of responders, DOR = 1.0).

E-G. Protein-protein interaction networks obtained from STRING [76] displaying the known interaction networks for three prominent CCIs *i.e.*, *GDF9* – *BMPR1B* (**E**), *NRTN* – *GFRA1* and *ARTN* – *GFRA1* (**F**) and *CX3CL1* – *CX3CR1* (**G**).

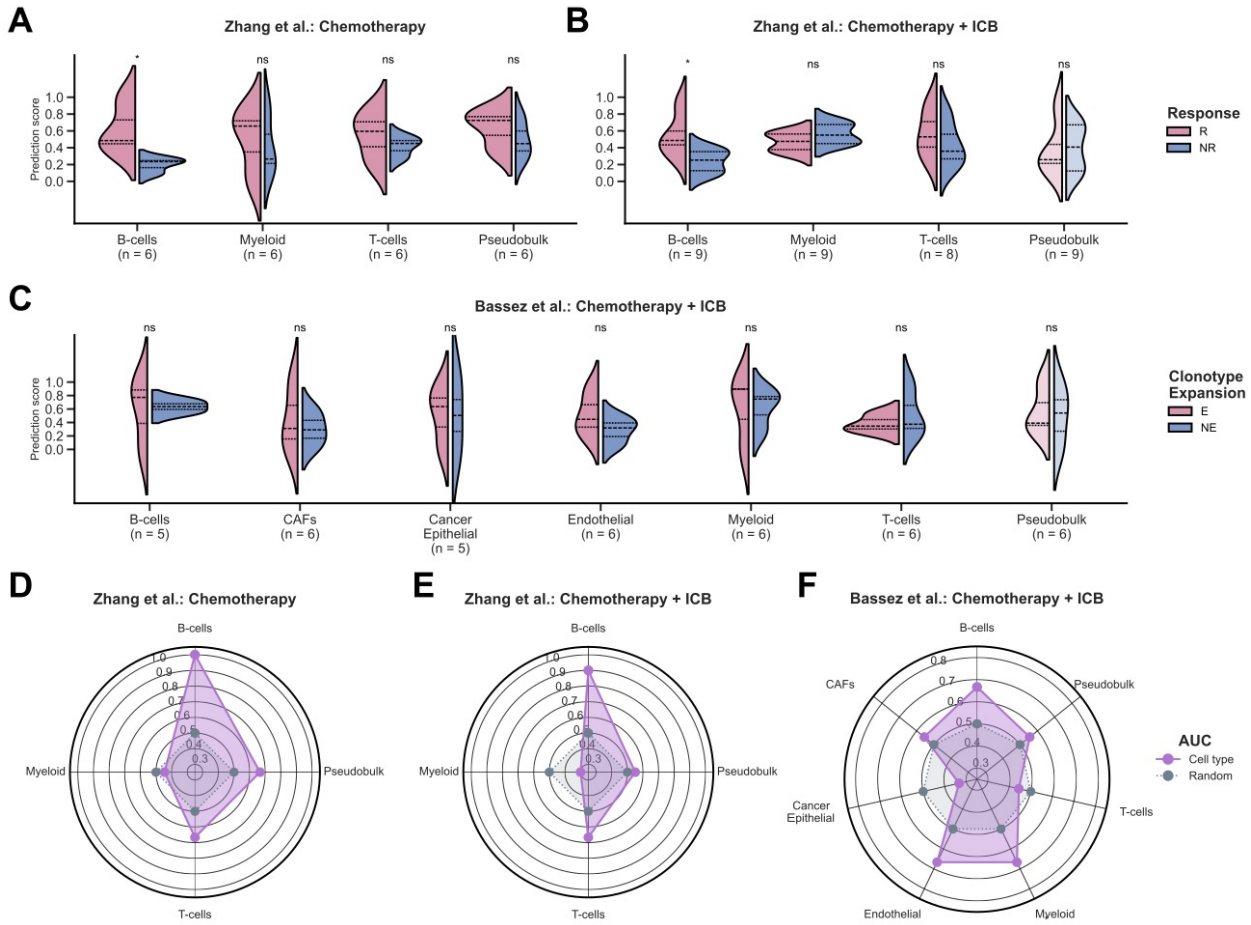

Supplementary Figure 7: DECODEM generalizes to single-cell (SC) transcriptomics for patient response prediction.

1337 **A-B.** Comparison of prediction scores for the cell-type-specific and pseudobulk (similar to bulk
1338 in previous scenarios) predictors across SC expression for predicting response to neoadjuvant
1339 chemotherapy (NAC) alone (**A**) or in combination with immune checkpoint blockade
1340 (ICB) therapy (**B**) from Zhang et al., or predicting T-cell clonotype expansion following treatment
1341 with NAC and ICB therapy (**C**) from Bassez et al. R, NR, E and NE stand for responders, non-
1342 responders, expanders and non-expanders, respectively. The differences between the
1343 prediction scores were computed by using a one-tailed Wilcoxon rank-sum test (* and 'ns'
1344 denote $P \leq 0.05$ and $P > 0.05$, respectively).
1345 **D-F.** Comparison of model performance for the cell-type-specific and pseudobulk predictors for
1346 predicting response to NAC alone (**D**) or in combination with ICB therapy (**E**) from Zhang et al.,
1347 and for predicting T-cell clonotype expansion following treatment with NAC and ICB therapy
1348 from Bassez et al. (**F**). AUC stand for the area under the receiver operating characteristics curve.
1349 'Random' denotes a random predictor (AUC = 0.5).
1350

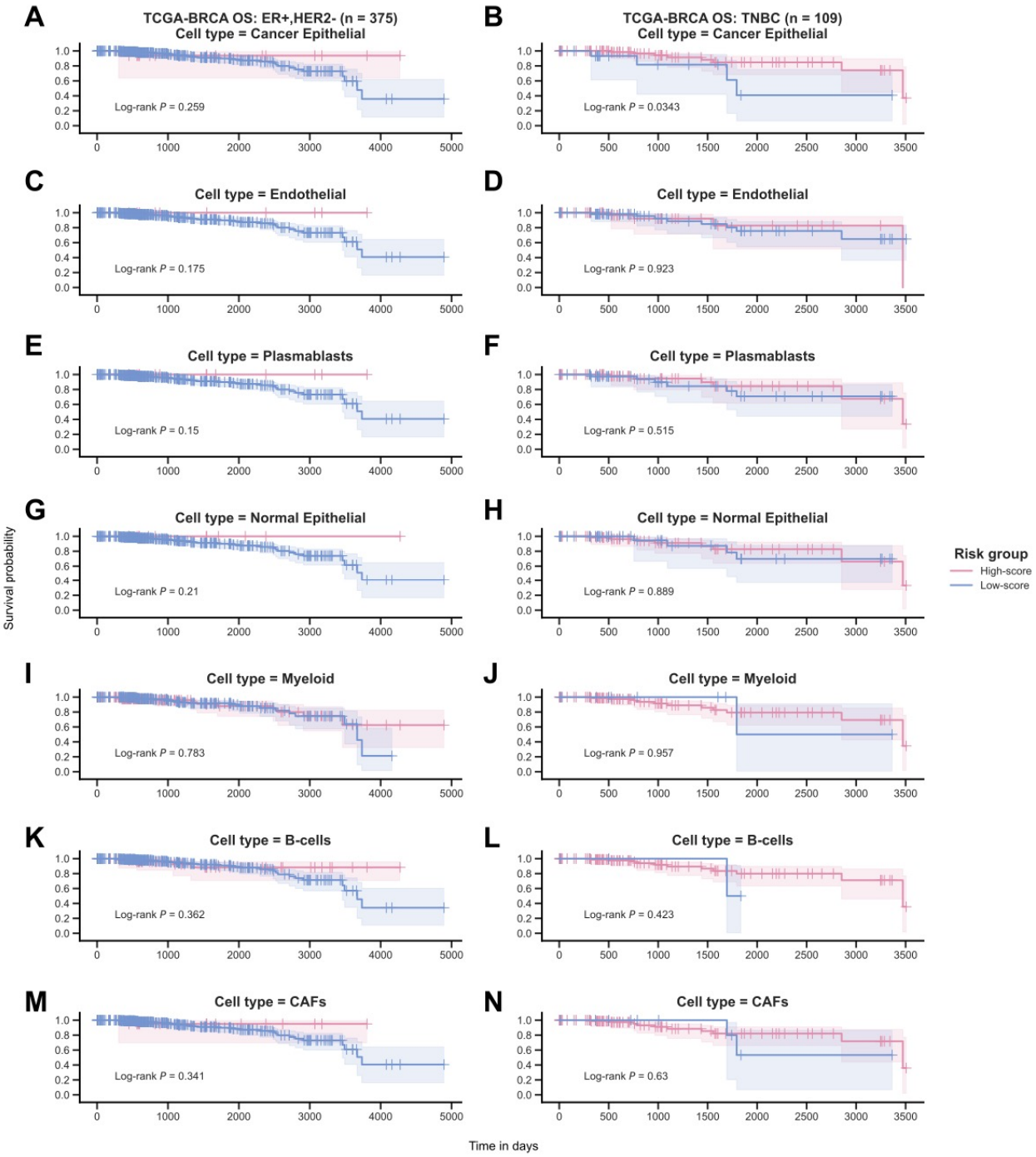

Supplementary Figure 8: The generalizability of DECODEM to the stratification of TCGA-BRCA overall survival (OS).

A-N. Kaplan-Meier curves depicting OS of early stage TCGA-BRCA patients with ER+,HER2- BC (**left**) and TNBC (**right**), stratified by DECODEM scores for seven prominent cell types. Patients were stratified into 'High-score' and 'Low-score' groups using a threshold of 0.5 on their

DECODEM scores for these seven cell types. The differences between the curves were computed by using a Log-rank test.

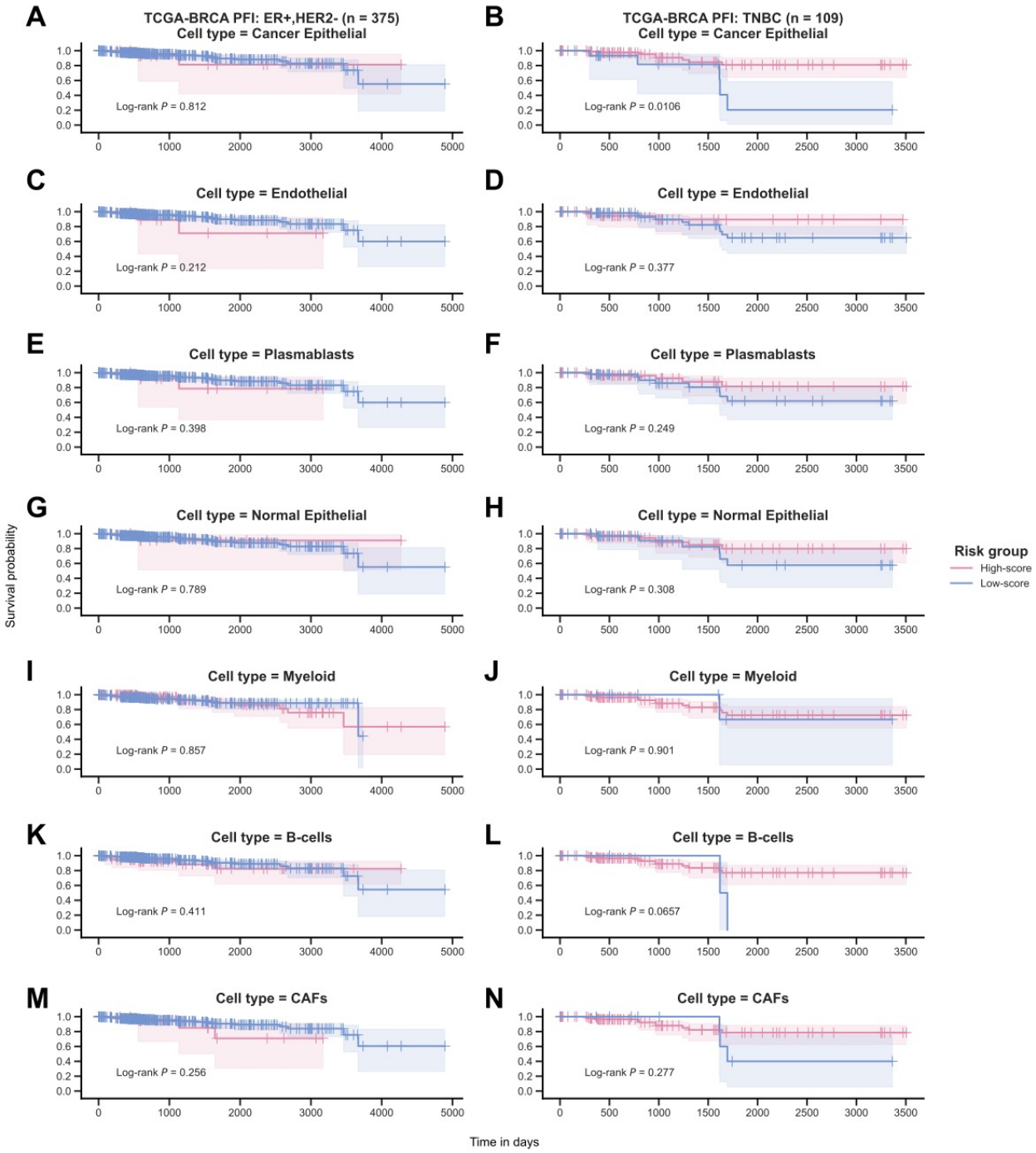

Supplementary Figure 9: The generalizability of DECODEM to the stratification TCGA-BRCA progression-free interval (PFI; synonymous to progression-free survival).

1363 **A-N**. Kaplan-Meier curves depicting PFI of early stage TCGA-BRCA patients with ER+,HER2- BC
1364 (**left**) and TNBC (**right**), stratified by DECODEM scores for seven prominent cell types. Patients
1365 were stratified into 'High-score' and 'Low-score' groups using a threshold of 0.5 on their
1366 DECODEM scores for these seven cell types. The differences between the curves were
1367 computed by using a Log-rank test.
1368